

Individual foraminiferal analysis: A promising tool for high-resolution temperature and pH reconstruction

Zifei Yang^{a,*}, Christopher D. Standish^a, Rachel M. Brown^{a,b}, Patrick A. Rafter^c, Malcolm B. Hart^d, Tali L. Babila^e, Gavin L. Foster^a

^a School of Ocean and Earth Science, University of Southampton, England, UK

^b Aix Marseille Université, CNRS, IRD, INRAE, Coll France, CEREGE, Aix-en-Provence, France

^c College of Marine Science, University of South Florida, Florida, USA

^d School of Geography, Earth and Environmental Sciences, University of Plymouth, England, UK

^e Department of Earth, Environmental and Planetary Sciences, Case Western Reserve University, OH, USA

ARTICLE INFO

Editor: Dr. Vasileios Mavromatis

Keywords:

Benthic foraminifera
Individual foraminifera analysis
El/Ca
 $\delta^{11}\text{B}$
Laser ablation
Western English Channel
Caribbean Sea
MC-ICP-MS/MS

ABSTRACT

Compared with traditional bulk foraminiferal analysis methods, in situ analysis of individual foraminiferal tests (individual foraminiferal analysis or IFA) offers several advantages over traditional bulk methods, including enhanced temporal resolution where fossiliferous sample material is limited as well as potentially resolving seasonal-scale climate variability in deep time. Despite these advantages, applications of element-to-calcium (El/Ca) ratios and $\delta^{11}\text{B}$ in benthic foraminifera using IFA remain limited, and the biogeochemical drivers of intra-test and inter-test geochemical variability are poorly constrained. In this study, we systematically evaluate El/Ca ratios and $\delta^{11}\text{B}$ in individual benthic foraminifera. By analysing Holocene epifaunal benthic foraminiferal species *Cibicoides wuellerstorfi* from a deep ocean core site (ODP Site 999), we conclude that intra- and inter-test variabilities are regulated by ontogenetic effects resulting in inter-test variabilities of ± 0.14 mmol/mol Mg/Ca, ± 14 $\mu\text{mol/mol}$ B/Ca, and ± 0.18 ‰ $\delta^{11}\text{B}$. Application of the IFA method to epifaunal benthic foraminifera species *Cibicides lobatulus* from a box core in the English Channel, UK reveals ~ 0.1 pH units acidification and ~ 1 °C warming since the mid-19th century. By demonstrating that individual-level variability in reconstructed temperature and pH tracks seasonal trends in the available contemporaneous water-column instrumental measurements at the same site, we provide a ground-truthing to our multi-proxy IFA methodology, and also demonstrate the potential for benthic IFA to provide seasonal-scale reconstructions of ocean climate over hundreds to millions of years.

1. Introduction

Benthic foraminifera are widely used in paleoceanographic reconstructions because the trace elements and isotopic composition of their calcite tests serve as important geochemical proxies for numerous aspects of Earth's past climate. Most notably, oxygen isotopes ($\delta^{18}\text{O}$) are used for global stratigraphy and deep ocean temperature reconstruction (e.g., Westerhold et al., 2020; Lisiecki and Raymo, 2005). Boron to Calcium (B/Ca) ratios and boron isotopic composition (expressed as $\delta^{11}\text{B}$) are applied to reconstruct the ocean carbonate system (e.g., Rae et al., 2011; Yu et al., 2010), while Magnesium to Calcium (Mg/Ca) ratios are used to estimate bottom water temperature (e.g., Lear et al., 2000). However, near-ubiquitous sediment mixing by benthic

macrofauna (a process known as bioturbation), together with sampling artefacts arising from bulk sampling of discrete sediment depths, can smooth paleoclimate records and dampen the magnitude of climate signals, potentially biasing paleoclimate reconstructions, particularly during abrupt and transient climate events (e.g., Hull et al., 2011; Kirtland Turner et al., 2017; Liu et al., 2021). For example, the abrupt ocean warming and acidification during Paleogene hyperthermals, such as the Paleocene-Eocene Thermal Maximum (PETM), present a particular challenge since they were geologically rapid, and often characterized by severe chemical erosion, limiting temporal resolution by insufficient calcareous microfossils for bulk analysis in most marine sedimentary sections (e.g., Babila et al., 2022; Tripathi and Elderfield, 2005). In situ single-test analysis of individual foraminifera (individual

* Corresponding author.

E-mail address: Zifei.Yang@soton.ac.uk (Z. Yang).

<https://doi.org/10.1016/j.chemgeo.2026.123395>

Received 25 November 2025; Received in revised form 18 March 2026; Accepted 24 March 2026

Available online 26 March 2026

0009-2541/© 2026 The Authors. Published by Elsevier B.V. This is an open access article under the CC BY license (<http://creativecommons.org/licenses/by/4.0/>).

foraminiferal analysis; IFA) can overcome limitations associated with traditional bulk sampling methods, not only because it requires smaller amounts of material compared to traditional solution-based analyses, but also because the variability among individual tests originating from different time intervals within a bioturbated sediment layer can be preserved. When interpreted together with sediment mixing models, IFA records can therefore provide additional constraints on true onset times and amplitudes of the underlying original climate signals (e.g., Dolman and Laepple, 2018; Hülse et al., 2022; Kirtland Turner et al., 2017). Moreover, monthly- to seasonal-scale snapshots of environmental conditions recorded by individual foraminiferal tests provide the opportunity to reconstruct seasonal climate amplitudes hundreds to millions of years ago. Such reconstructions are essential for constraining and validating climate model simulations, particularly for deep-time intervals where seasonal cycles in climate variables remain poorly understood (e.g., Huber and Caballero, 2011; Tierney et al., 2025; Tindall et al., 2022). Measurements of $\delta^{13}\text{C}$, $\delta^{18}\text{O}$, and Mg/Ca of individual planktic foraminifera have already been used either independently or in combination, to reconstruct decadal to centennial climate variability, and reveal climate variability occurring at timescales shorter than those averaged by typical multi-specimen foraminiferal samples (i.e. $\sim 1\text{--}5$ kyr; Inglis et al., 2023; Kozdon and Kelly, 2024; Thirumalai et al., 2013; Zachos et al., 2007). While most studies to date have focused on established proxy systems (see Fehrenbacher et al., 2024 for review), recent analytical advances (Fietzke and Anagnostou, 2023; Sadekov et al., 2019; Standish et al., 2019, 2025) have enabled measurement of $\delta^{11}\text{B}$ in individual foraminifera using laser ablation multi-collector inductively coupled plasma mass spectrometry (LA-MC-ICPMS; Babila et al., 2022; Coenen et al., 2024; Mayk et al., 2020; Raitzsch et al., 2020; Standish et al., 2019).

An emergent factor highlighted by a recent compilation of IFA studies is the consistently greater variability observed in geochemical measurements of individual foraminiferal tests compared to traditional bulk multi-specimen analyses (Fehrenbacher et al., 2024). Although the exact causes remain uncertain, this geochemical variability likely reflects a combination of environmental variability experienced during the life cycle of the foraminifera and/or individual-level “vital effects” — geochemical offsets from equilibrium driven by physiological processes related to biomineralisation and life function. While the mechanistic basis of vital effects are poorly understood (e.g., Branson and de Nooijer, 2025; de Nooijer et al., 2014; Erez, 1978), non-equilibrium elemental and isotopic behavior is well documented for oxygen, carbon and boron isotopes, as well as trace element incorporation into the calcite tests of foraminifera (e.g. Zeebe et al., 2008). For example, $\delta^{11}\text{B}$ in foraminifera has been widely applied as a proxy for seawater pH because foraminiferal $\delta^{11}\text{B}$ approximates the $\delta^{11}\text{B}$ of seawater borate, which is largely a function of ambient ocean pH (see Foster and Rae, 2016 for review). However, in benthic foraminifera, microhabitat environmental conditions in addition to bottom water ocean pH can influence test $\delta^{11}\text{B}$ values (e.g. Rae et al., 2011). Boron isotopes of infaunal benthic foraminifera species do not simply reflect bottom water chemistry but vary relative to porewater pH and $\delta^{11}\text{B}$ porewater composition that may differ from overlying seawater values (e.g. Rae et al., 2011). Beyond habitat-related complications, foraminiferal vital effects in $\delta^{11}\text{B}$ are thought to arise from photosynthesis of symbiotic algae, respiration, and calcification processes, all of which modify microenvironmental pH around a living foraminifer and can introduce isotopic offsets between calcite $\delta^{11}\text{B}$ and seawater borate $\delta^{11}\text{B}$ (e.g., Coenen et al., 2024; Rae et al., 2011; Rollion-Bard and Erez, 2010). To fully interpret IFA data, the degree of geochemical variability caused by vital effects must be quantified.

Although habitat-related and life processes can cause disequilibrium effects in $\delta^{11}\text{B}$ of infaunal benthic foraminifera (e.g., Rae et al., 2011) and symbiont bearing species (e.g., Rollion-Bard and Erez, 2010), the influence of such vital effects is likely minimised in individual analysis of non-symbiont bearing epifaunal benthic foraminifera. Indeed, Rae

et al. (2011) using traditional multi-specimen $\delta^{11}\text{B}$ solution analysis showed that epifaunal foraminiferal $\delta^{11}\text{B}$ closely tracks seawater borate $\delta^{11}\text{B}$. Nevertheless, IFA studies have reported substantial intra-test variability in the epibenthic species *Cibicidoides wuellerstorfi*. Raitzsch et al. (2020), using IFA via LA-MC-ICPMS reported an averaged intra-test $\delta^{11}\text{B}$ variability of 1.3 ‰ for the epibenthic *C. wuellerstorfi*, and a decreasing trend of more than 0.5 ‰ from the final chamber to the f-6 chamber (the seventh chamber from the aperture) in the final whorl, based on two individuals, and Sadekov et al. (2019) noted a $\sim 2\%$ decrease along the last whorl in the one individual analysed. Similarly, Raitzsch et al. (2011) using IFA via laser ablation ICPMS reported substantial intra-test variability of B/Ca and Mg/Ca in *C. wuellerstorfi*, reporting higher B/Ca and lower Mg/Ca ratios in the final chamber, with intra-test heterogeneities of $\pm 43\%$ and $\pm 51\%$ respectively. If these intra-test variations in $\delta^{11}\text{B}$, B/Ca and Mg/Ca in *C. wuellerstorfi*, a deep-sea species (Holbourn et al., 2013), were solely attributable to environmental conditions experienced during the life cycle, they would equate to changes in seawater pH, ΔCO_3^{2-} and temperature of $\sim 0.05\text{--}0.2$ pH units, ~ 54 $\mu\text{mol}/\text{kg}$ and ~ 2 °C respectively (calibration methods in section 2.5). These variations exceed typical deep-sea oceanographic environmental variability, underscoring the need to constrain the potential impact of vital effects on intra-test foraminiferal geochemical composition. In addition to this intra-test variability, Raitzsch et al. (2020) also observed ± 1.6 ‰ (2SD, $n = 18$) $\delta^{11}\text{B}$ variability between individuals of *C. wuellerstorfi*. In contrast, Standish et al. (2019) found that eight *C. wuellerstorfi* tests were indistinguishable and within analytical uncertainty (± 0.48 ‰, 2SD, $n = 9$), implying that differences in analytical techniques and instrumentation may contribute to the currently observed inter- and intra-test variability in $\delta^{11}\text{B}$ of modern *C. wuellerstorfi*.

Here we utilize recent advances in mass spectrometry and present the first IFA $\delta^{11}\text{B}$ analysis of benthic foraminifera collected by LA-MC-ICPMS/MS through the use of a Thermo Scientific Neoma MS/MS mass spectrometer (hereafter LA-Neoma). Key benefits of this approach over previous analytical set-ups are increased sensitivity (e.g. $\sim 1.4\times$ more sensitive compared to a Neptune MC-ICPMS; Standish et al., 2025), and removal of a spectral interference from scattered ions seen on pre-existing models of MC-ICPMS when ion detection employs Faraday cup detectors rather than ion counters (Fietzke and Anagnostou, 2023; Sadekov et al., 2019; Standish et al., 2019), thus permitting accurate measurement of higher and more stable signals (Standish et al., 2025). First, cleaning protocols for IFA benthic foraminifera are optimized to maximise cleaning efficiency while minimizing sample loss for paired analyses of $\delta^{11}\text{B}$, Mg/Ca and B/Ca. Vital effects in individual benthic foraminifera are then evaluated by characterization of intra- and inter-test geochemical variability in a modern deep-sea site. Finally, the updated cleaning protocol and analytical method is applied to downcore sediments from a continental shelf environment in the English Channel to ground-truth the reliability of the approach by comparing contemporaneous hydrographic observations to geochemical reconstructions, revealing the overall trends and seasonal variations in seawater temperature and pH over the last 150 years in the coastal UK.

2. Material and methods

2.1. Sediment material and benthic foraminifera species

The sediment material analysed here comes from two different oceanic locations. An early Holocene sample is used from ODP Site 999, located in the Colombian Basin, Caribbean Sea ($12^\circ 44.639'\text{N}$, $78^\circ 44.360'\text{W}$) with a water depth of 2828 m. The age of the studied sediment layer is dated at 9.28 ka based on oxygen isotope stratigraphy (Schmidt et al., 2004). In addition, sediment samples were recovered from two Western Channel Observatory (WCO; <https://www.westernchannelobservatory.org.uk/>) sites located in the English Western Channel managed by Plymouth Marine Laboratory (Fig. S1). Site L4 ($50^\circ 15.00'\text{N}$,

4°13.02'W) has a water depth of 50 m, while the Cawsand site (CS; 50°19.81'N, 4°11.45'W) is shallower, at approximately 10 m. A surface sediment sample was collected from CS, and a sediment core was collected from L4 (three depth intervals: 0–2 cm, 12–15 cm and 25–30 cm) in June 2016.

All sediment samples were washed through a 63 µm sieve, and benthic foraminifera were picked from the >212 µm coarse fraction. Glassy tests of *C. wuellerstorfi* were picked from ODP Site 999, and *C. lobatulus* from the WCO sites, under a binocular microscope. At WCO sites CS and L4, *Ammonia* spp., *Elphidium crispum* and *C. lobatulus* are the most abundant calcareous species (Hart et al., 2016). *C. lobatulus* was selected for this study because it is genetically related to the cosmopolitan and commonly used paleoceanographic benthic foraminifera species *C. wuellerstorfi* (Schweizer et al., 2009) and it calcifies throughout the year in all seasons (Manley, 1997; Wisshak and Rüggeberg, 2006). As an epiphytic 'type B' species defined by Langer (1993), *C. lobatulus* has a lifespan of approximately 2–5 months, enabling each test to record sub-seasonal to multi-seasonal variability that may span up to three adjacent seasons. These characteristics make *C. lobatulus* well suited for reconstructing past seasonal variations in water properties in the English Western Channel.

All specimens analysed by LA-ICPMS were assigned to an individual identifier and weighed by microbalance (Sartorius ME-5; d = 0.001 mg). Specimens were photographed using Leica M205C stereo microscope with IC90HD camera illuminated from above. Images were analysed by Image Pro Premier to calculate the 2D surface area for each individual.

2.2. Sample preparation

2.2.1. IFA specimens

It is desirable for in situ IFA to preserve the foraminiferal test whole, however, ultrasonication, the preferred method to remove clay contamination (Barker et al., 2003), frequently led to unacceptable amounts of test breakage. We therefore sought to develop a suitable approach to physical cleaning that minimises test breakage and yet maximises contaminant removal. To achieve this, we carried out a series of cleaning tests on *C. wuellerstorfi* from ODP 999 and *C. lobatulus* from WCO CS, by analysing in situ El/Ca ratios (including contamination indicators, Al/Ca, Mn/Ca, and Fe/Ca) and $\delta^{11}\text{B}$ of specimens cleaned using different protocols. The details of these cleaning tests can be found in Supplementary Information 2 or SI2. The results of the cleaning tests indicate that physical and chemical cleaning combined with strict data screening on time-resolved measurements can effectively reduce contamination for El/Ca and $\delta^{11}\text{B}$ (SI2). Following this investigation, data reported in the main text for *C. wuellerstorfi* from ODP 999 (12 individuals) and *C. lobatulus* from WCO CS (18 individuals) were cleaned following the protocol adapted from Barker et al. (2003) and Babila et al. (2022), including clay removal (ultrasonication in methanol or methanol rinsing without ultrasonication to avoid test breakage), and oxidative cleaning (details in SI2). Specimens from the WCO L4 sediment core (more than 12 individuals each interval) were all cleaned with ultrasonication during the clay-removal step. All cleaned specimens were mounted on double-sided tape with the umbilical side facing upward.

2.2.2. Bulk solution samples

Four samples from both WCO sites and ODP Site 999 were also analysed by solution methods. Samples for bulk solution analysis were cleaned following the protocol of Barker et al. (2003). Approximately 20 specimens of *C. wuellerstorfi* and *C. lobatulus* (~0.4 mg) were crushed between pre-cleaned glass slides to open all chambers. Potential clay infilling was removed by 4 × 20s ultrasonication in Milli-Q water, while organic contamination was removed by an oxidative step using an oxidative mixture (30 × dilution of 30% H₂O₂ buffered with 0.1 M NH₄OH). A final weak acid leaching step (0.005 M HNO₃) was conducted to remove potential contamination reabsorbed to the test surface

following solubilisation during prior cleaning steps. Clean samples were then dissolved by the stepwise addition of 0.5 M HNO₃, with 20 µl aliquots taken for El/Ca ratios (Mg/Ca, B/Ca, Al/Ca, Mn/Ca etc.) and the remainder subjected to the batch purification technique for B separation described in Trudgill et al. (2024).

2.3. Analyses techniques

2.3.1. In situ El/Ca

In situ El/Ca ratios were determined by laser ablation triple quadrupole inductively coupled plasma-mass spectrometer (LA-QQQ-ICP-MS, abbreviated hereafter as LA-QQQ) in the Centre for Earth Analysis and Research Southampton (CERAS) housed at the University of Southampton, using an Agilent 8900 QQQ-ICP mass spectrometer (Agilent Technologies Inc., CA, USA) coupled to an Elemental Scientific Lasers (Bozeman, MT, USA), New Wave Research 193 nm excimer laser ablation system with a TwoVol2 ablation chamber. Analytical methods followed Standish et al. (2024), and operating conditions are detailed in Table S1. Primary glass reference materials included NIST SRM610 and NIST SRM612 and carbonate materials JCp-1 (*Porites* sp., deep-sea coral) and Jct-1 (*Tridacna gigas*, bivalve). In-house carbonate material PS96/381-1b, a fragment of deep-sea coral was used as a secondary standard and was ablated throughout the analytical session to assess analytical precision and accuracy. The preparation and detailed information of all the reference materials can be found in Standish et al. (2019, 2024).

Mounted benthic foraminiferal individuals and standards were analysed for B, Mg, Al, Ca, Mn, Fe and Sr, with Al, Mn and Fe used to specifically monitor clay and other sediment-derived contamination. A circular laser beam was used with a diameter of 35 µm, a laser repetition rate of 5 Hz, and a laser power density of 1 J/cm². 60s dwell times were used to ensure that the laser ablated through the chamber walls. A 30s washout delay, that served as a blank measurement was carried out between each 60s ablation. Blank corrections were applied based on an average of the preceding and succeeding blank measurements. The ablation spots were targeted on the chambers of the final whorl, from the final chamber (f) to the penultimate chambers (f-n). Reference materials (three analyses of each) were analysed after every 20 sample analyses. After completing analysis, raw datasets were reduced using Iolite4 with the 3D Trace Element data reduction scheme (Paton et al., 2011). Long-term reproducibility of reference material PS96/381-1b throughout the analytical sessions was 3.0 ± 0.4 µmol/mol Sr/Ca, 39.72 ± 5.75 µmol/mol Li/Ca, 79.8 ± 10.56 mmol/mol Mg/Ca and 236 ± 31.24 µmol/mol B/Ca (2SD), which are consistent with solution values (Sr/Ca 2.9 ± 0.03 µmol/mol, Li/Ca 48.67 ± 10.79, Mg/Ca 78.97 ± 2.71 mmol/mol and B/Ca 233.82 ± 44.77 µmol/mol; ± 2SE; Standish et al., 2024). The accuracy of absolute values of Al/Ca, Mn/Ca and Fe/Ca analysed by LA-QQQ cannot be demonstrated and as such are only used here to evaluate the effectiveness of the cleaning protocols and for screening data for contamination.

2.3.2. In situ $\delta^{11}\text{B}$

After analysis by LA-QQQ, the same samples were analysed for in situ $\delta^{11}\text{B}$ by LA-Neoma at CERAS using a Thermo Scientific Neoma MS/MS MC-ICP mass spectrometer (Thermo Fisher Scientific, Waltham, MA, USA) coupled to an Elemental Scientific Lasers (Bozeman, MT, USA) New Wave Research 193 nm excimer laser ablation system with a TwoVol2 ablation chamber. The analytical methods closely followed Standish et al. (2025). By eliminating interference from scattered ions of Ca and Ar using the mass spectrometer's pre-cell mass filter, the Neoma improves analytical accuracy for $\delta^{11}\text{B}$ when ion detection employs Faraday cup detectors compared to pre-existing models of MC-ICP mass spectrometers (see Standish et al., 2025). Glass reference materials NIST SRM610 and carbonate reference materials JCp-1 and inorganic calcite UWC-1 (inorganic calcite nanopowder pellet) were used as primary standards. In-house carbonate material reference material PS96/381-1b

was used as a secondary standard. All the reference materials were ablated throughout the analytical sessions. The preparation and detailed information of all the reference materials can be found in (Standish et al., 2024, 2025).

Samples and reference materials were simultaneously analysed for ^{10}B and ^{11}B on the L5 and C Faraday cups respectively with ^{12}C measured on the H5 Faraday cup. Operating conditions are detailed in Table S2. A circular laser beam with a diameter of $100\ \mu\text{m}$ was used with a 10 Hz repetition rate and laser power density of $3.5\ \text{J}/\text{cm}^2$. Dwell times of 20s were used to ensure that the laser fully ablated through the chamber walls, with blanks characterised over the preceding 5 s and succeeding 15 s (20s in total). Integration times of 0.1 s were employed. The ablation spots were targeted on each chamber beside the ablation crater of the previous El/Ca analysis, from the final chamber (f) to the penultimate chambers (f-n), including the umbo. Because of the larger spot size for $\delta^{11}\text{B}$ analysis, not all chambers were able to accommodate a spot of $100\ \mu\text{m}$. The aforementioned reference materials (three analyses of each standard) were analysed after every 20 sample ablations. After the completion of the analytical sequences, raw datasets were reduced on Iolite4 using a custom-made data reduction scheme (DRS) “B_Neoma” (Standish et al., 2025). On-peak blank corrections were applied to each measured mass cycle by cycle following smoothing of the blank intensities using a spline function (“Smooth9”). Instrumental mass bias was corrected by normalising to NIST SRM610 glass reference material using a spline function (“Smooth9” spline). Finally, secondary normalisation to carbonate reference materials JCp-1 and UWC using a two-point linear calibration was applied. Repeat analysis of secondary reference material PS96/381-1b gave a reproducibility of $\pm 1.3\ \text{‰}$ (2SD, $n = 78$), with a mean $\delta^{11}\text{B}$ of $15.36 \pm 0.15\ \text{‰}$ (2SE, $n = 78$; SE = SD/\sqrt{n} , and see Section 2.4.2 for detailed explanation), which compares well with the solution value of $15.25 \pm 0.27\ \text{‰}$ (2SD).

2.3.3. Bulk solution El/Ca and $\delta^{11}\text{B}$

Bulk El/Ca ratios of solutions were analysed by High Resolution ICP-Mass Spectrometer (Thermo Finnigan Element XR) at the CERAS facility,

using Ca concentration matched standards to reduce matrix effects following Lear et al. (2010). Analytical reproducibility of consistency standards for Li/Ca, B/Ca, Mg/Ca, Al/Ca, Mn/Ca and Sr/Ca is 12%, 8%, 5%, 14%, 10% and 8% (2SD) respectively.

Solution $\delta^{11}\text{B}$ was measured at the CERAS facility using a Thermo Scientific Neptune multicollector inductively coupled plasma mass spectrometer (MC-ICPMS), following established methods (Foster et al., 2013). The long-term external reproducibility based on repeat measurements of JCp-1 is $24.2 \pm 0.20\ \text{‰}$ (2SD), consistent with the inter-lab value of $24.25 \pm 0.22\ \text{‰}$ (2SD) (Gutjahr et al., 2021). Each solution sample was analysed 3 times, when the triplicate standard deviation was larger than $0.20\ \text{‰}$, the standard deviation of triplicate was reported, otherwise the long-term reproducibility was reported.

2.4. Data processing

2.4.1. Data screen for time-resolved measurements

To monitor potential contamination on the exterior surface and clay mineral infilling, oxidative coatings, etc., Al, Mn, Fe intensities were used to screen all the time-resolved data of each LA-QQQ measurement. Elevated counts of Al, Mn, Fe at the beginning of the ablation and immediately before ablating through the chamber, which are usually accompanied by elevated Mg/Ca, Li/Ca and B/Ca ratios, were identified as contaminated signals (Fig. 1a). Similar to LA-QQQ measurements, time-resolved results of LA-Neoma have also been carefully screened, with declining $^{11}\text{B}/^{10}\text{B}$ ratios accompanied by increased ^{11}B and $^{11}\text{B}/^{12}\text{C}$ ratios identified as potential contamination (Fig. 1b). The contaminated signals were discarded before performing data reduction.

2.4.2. Standard deviation and standard error

In this study, both standard deviation (SD) and standard error (SE) were used to describe the uncertainty of the data presented, where $\text{SE} = \text{SD}/\sqrt{n}$ ($n = \text{number of individuals}$). The standard deviation is used as a measure of variability about the mean, while standard error is an estimate of the uncertainty on the mean (Altman and Bland, 2005). After

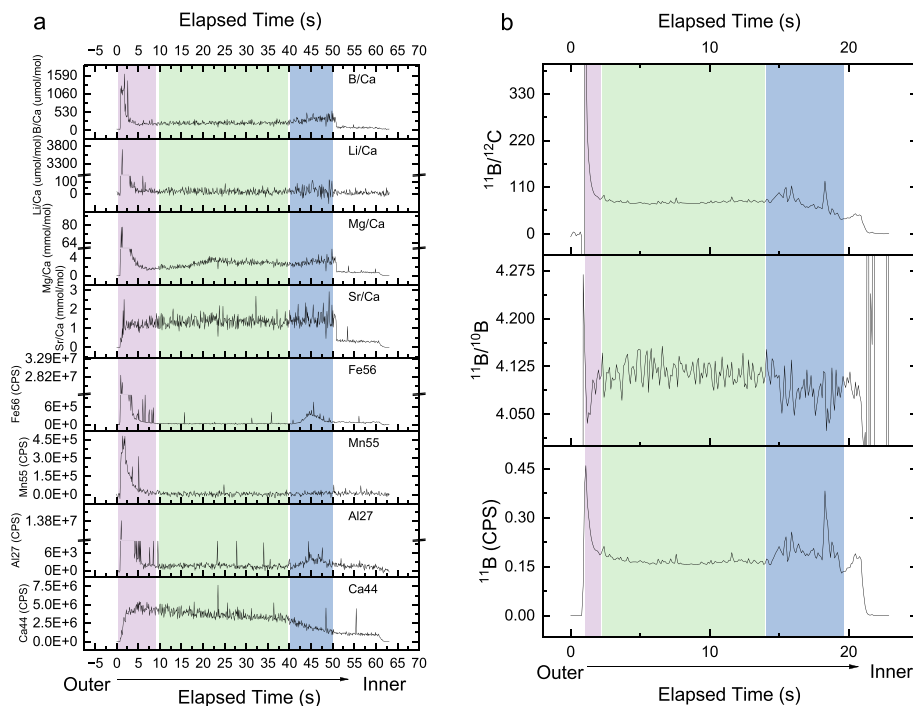


Fig. 1. Examples of depth-profile time-resolved measurements for a. El/Ca ratios, b. boron isotopes. Al, Mn, and Fe were used to screen for contamination. Violet bands indicate signals affected by exterior contamination, green bands indicate signals from calcite walls, and blue bands indicate signals affected by interior contamination. Only signals showing no evidence of contamination (highlighted by green bands) were selected during data screening. Ablation proceeds from the exterior to the interior. (For interpretation of the references to colour in this figure legend, the reader is referred to the web version of this article.)

screening the data of each ablation measurement, mean \pm 2SE were used in subsequent data interpretation. Within each individual, SD and SE were calculated with the average of every chamber ablation measurement used to quantify the intra-test variability and appropriate mean values of each test respectively. Among the individuals, SD and SE were calculated with the average values of tests to understand the inter-test variability and to estimate mean values of the populations, which are then compared with data from bulk solution methods.

2.5. Mg/Ca-temperature and $\delta^{11}\text{B}$ -pH calibration

For Mg/Ca, different temperature calibration equations were applied to the data generated at ODP Site 999 for *C. wuellerstorfi* and WCO sites for *C. lobatulus*, since the two locations experienced contrasting ranges of bottom water temperature (BWT): ODP Site 999 has a modern BWT of $\sim 3.85^\circ\text{C}$ at 2828 m (Johnson and Purkey, 2009), while the BWT at WCO stations seasonally varies between 7 and 18°C (McEvoy et al., 2023). It has been previously reported that the temperature sensitivity of benthic foraminiferal Mg/Ca varies across the range of typical habitat conditions linked, at least in part, to carbonate system effects arising from the coupling of low carbonate saturation and low temperature in the cold deep sea (Elderfield et al., 2006). Carbonate saturation effects on Mg/Ca were not corrected for in this study, as $\Delta[\text{CO}_3^{2-}]$ values at WCO L4 are typically $>80\ \mu\text{mol/kg}$ (McEvoy et al., 2023; Fig. S2), and at ODP 999 are $\sim 120\ \mu\text{mol/kg}$ (9.6 ka; Yu et al., 2010), indicating high-saturation environments at both locations. Under these conditions, carbonate saturation effects on Mg/Ca are not expected to represent first-order control (Yu and Elderfield, 2008). Accordingly, Mg/Ca ratios of the *C. lobatulus* measured here were converted into BWT using $\text{Mg/Ca} = 0.731 \pm 0.072 \exp. (0.123 \pm 0.007 \times \text{BWT})$, which is based on *Cibicides* spp. and *C. lobatulus* from core-top samples from the Nordic Seas, the Western Atlantic and the Indian Ocean with temperatures ranging from 4 to 19°C (Fig. S3). The original data for this calibration are from Elderfield et al. (2006), Marchitto et al. (2007), and Quillmann et al. (2012). The combined uncertainty in BWT derived by the calibration and the analytical uncertainty of laser ablation method is $\sim 2^\circ\text{C}$ (2SD). The Mg/Ca-temperature calibration equation for *C. wuellerstorfi* applied in this study is in the $<4^\circ\text{C}$ range: $\text{Mg/Ca} = 0.781 \pm 0.023 \exp. (0.23 \pm 0.013 \times \text{BWT})$ (Healey et al., 2008). The combined uncertainty in BWT using this calibration is $\sim 0.6^\circ\text{C}$ (2SD).

The calculation of seawater pH from *C. lobatulus* and *C. wuellerstorfi* $\delta^{11}\text{B}$ followed Foster and Rae (2016). As indicated by Rae et al. (2011), the $\delta^{11}\text{B}$ values of epifaunal benthic foraminifera agree with $\delta^{11}\text{B}$ values of seawater $\text{B}(\text{OH})_4^-$, which is determined predominantly by seawater pH (Foster and Rae, 2016), allowing pH to be determined from foraminiferal $\delta^{11}\text{B}$ by the following equation:

$$\text{pH} = \text{p}K_B^* - \log \left(\frac{\delta^{11}\text{B}_{\text{SW}} - \delta^{11}\text{B}_{\text{CaCO}_3}}{\delta^{11}\text{B}_{\text{SW}} - \alpha_B \times \delta^{11}\text{B}_{\text{CaCO}_3} - \varepsilon_B} \right)$$

where K_B^* is dissociation constant for boric acid, calculated here using the 'Seacarb' R package (Gattuso et al., 2021), using the temperature derived from foraminiferal Mg/Ca, an average salinity of 35.2 from the 2008–2016 CTD time-series record at WCO Site L4 with a water depth of 50 m (McEvoy et al., 2023), and 34.9 at ODP Site 999 assuming no major variation of salinity during the Holocene at Caribbean Sea (Gallegos, 1996); $\delta^{11}\text{B}_{\text{SW}} = 39.61$ (Foster et al., 2010), $\alpha_B = 1.0272$ (Klochko et al., 2006), and $\varepsilon_B = (\alpha_B - 1) \times 1000$. A Monte Carlo approach was used to propagate uncertainties in K_B^* which mainly arise from Mg/Ca derived temperature, and in IFA $\delta^{11}\text{B}_{\text{carbonate}}$, yielding a typical uncertainty in derived pH of ~ 0.12 pH units at 95% confidence.

2.6. Dating of WCO Site L4

Radiocarbon content ($^{14}\text{C}/\text{C}$) and $\delta^{13}\text{C}$ of *C. lobatulus* at WCO L4 were used to estimate sample ages. The $^{14}\text{C}/\text{C}$ was analysed by

accelerator mass spectrometer at the University of California, Irvine, and calibrated using OX1 primary standards following the conventions of Santos et al. (2007) and Southon et al. (2004). By assuming that *C. lobatulus* specimens in the 0–2 cm layer were deposited shortly before core collection in 2016 CE, and the resulting local reservoir age was used to determine the calendar ages of deeper samples.

Ten *C. lobatulus* tests from 212 to 250 μm size fraction were homogenized, and $\sim 50\ \mu\text{g}$ was analysed for $\delta^{13}\text{C}$ by Thermo Scientific Kiel IV Carbonate device coupled with a MAT253 isotope ratio mass spectrometer in the SIRMS Laboratory at University of Southampton. Reference materials NBS-18 (IAEA, Vienna, Austria; $\delta^{13}\text{C} = -5.01\ \text{‰}$) and GS1 (in-house standard; Carrara Marble; $\delta^{13}\text{C} = 2.16\ \text{‰}$) were analysed with the samples as external standards, the $\delta^{13}\text{C}$ data were then normalized by two-point calibration, and reported relative to Vienna PeeDee Belemnite. The analytical uncertainty is $0.03\ \text{‰}$. The *C. lobatulus* $\delta^{13}\text{C}$ values were compared to regional high-resolution Northwest Atlantic foraminifera $\delta^{13}\text{C}$ record spanning last 4000 yrs. (Mellon et al., 2019), that displays a pronounced $\delta^{13}\text{C}$ Suess effect.

3. Results

3.1. Comparison of IFA and bulk solution

Mean IFA values of Mg/Ca, Sr/Ca, B/Ca and $\delta^{11}\text{B}$ are compared with results generated by the bulk solution method in Fig. 2 and Table 1. Mg/Ca, Sr/Ca and $\delta^{11}\text{B}$ ratios generated by the two methods are in good agreement (Fig. 2, Table 1). B/Ca ratios generated by IFA methods agree with solution results at ODP Site 999, while the means measured by LA-QQQ are generally higher than the solution data for the samples from the WCO stations by around 17% (Fig. 2, Table 1). This is marginally higher than our uncertainty bounds ($\pm 13\%$) based on repeat analysis of our secondary ablation standards, and its origin therefore remains uncertain but systematic offsets between results generated from laser ablation and solution-based methods have been reported previously for foraminifera, arising from differences in sampling strategy and test heterogeneity, even when analytical precision are comparable between methods (e.g., Fehrenbacher et al., 2020). Such effects are expected to be especially relevant for elements whose incorporation is strongly modulated by biological processes and calcifying fluid chemistry, such as boron. Given these uncertainties, discussion of the absolute B/Ca values derived from LA-based IFA at the WCO stations is therefore limited to relative intra- and inter-test patterns rather than absolute values. B/Ca values of *C. wuellerstorfi* generated here by both IFA ($239 \pm 14\ \mu\text{mol/mol}$ at 9.28 ka, 2SE) and solution ($229 \pm 21\ \mu\text{mol/mol}$ at 9.28 ka, 2SD) methods are broadly consistent with the published ODP Site 999 solution-based data of similar age by Chalk et al. (2019; $214 \pm 13\ \mu\text{mol/mol}$ at 9.5 ka, 2SD). Our ODP 999 $\delta^{11}\text{B}$ values also agree with solution-based result of samples of a similar age from an adjacent site VM28–122 (Yu et al., 2010; $16.85 \pm 0.25\ \text{‰}$ at 9.6 ka vs. IFA: $16.71 \pm 0.18\ \text{‰}$ or solution: $16.66 \pm 0.25\ \text{‰}$ at 9.28 ka here).

Given the numbers of specimens analysed in this study (typically ~ 12 individuals per sample), the standard errors on the IFA mean values are also comparable with the uncertainty of solution-based analyses (Table 1). Following the standard error calculation equation ($\text{SE} = \text{SD}/\sqrt{n}$), a reduction in the number of individuals analysed would lead to a predictable increase in uncertainty (e.g. halving the number of specimens from 12 to 6 would increase the uncertainty by a factor of $\sqrt{2}$).

3.2. Intra- and inter-test variabilities

Specimens from ODP Site 999 exhibit lower intra-test variabilities for Sr/Ca and $\delta^{11}\text{B}$, and lower inter-test variabilities for Mg/Ca and $\delta^{11}\text{B}$, than those from the WCO stations (Table 1, Fig. 3). In contrast, intra-test variability of Mg/Ca and B/Ca and inter-test variability of Sr/Ca and B/Ca are broadly similar between the two locations (Table 1, Fig. 3).

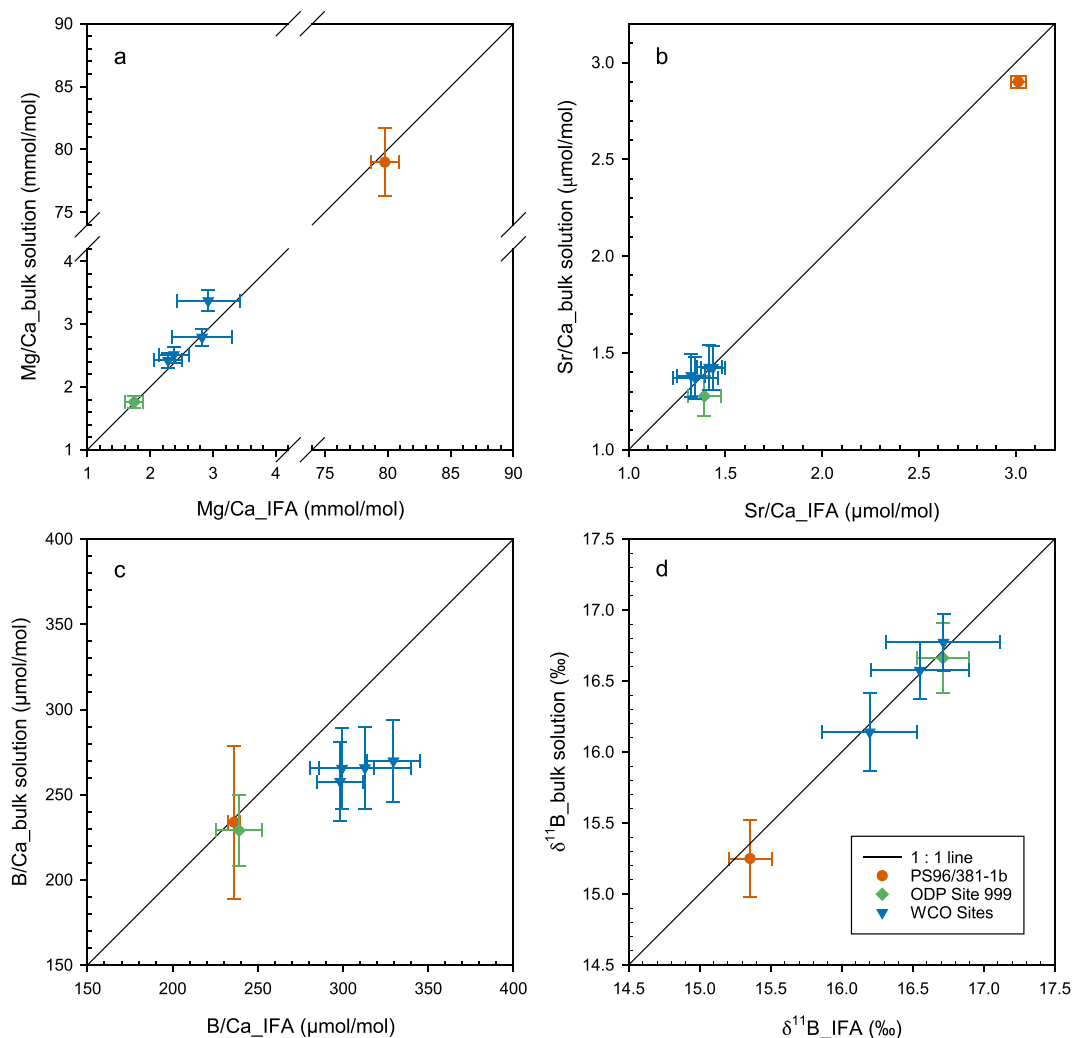


Fig. 2. Comparison of IFA values versus solution values of a. Mg/Ca, b. Sr/Ca, c. B/Ca and d. $\delta^{11}\text{B}$. ODP Site 999 is represented by the benthic foraminifera species *C. wuellerstorfi* and WCO by *C. lobatulus* (see Fig. S1 for map location). PS96/381-1b is an in-house carbonate material (deep-sea coral) used as secondary standard.

Within specimens from the WCO sites, no consistent trends are observed in Sr/Ca, Mg/Ca, B/Ca, and $\delta^{11}\text{B}$ from f to f-n chambers along the final whorl (Fig. 3 and Fig. S4). In contrast, specimens from ODP Site 999 display systemic increases in Sr/Ca and Mg/Ca and $\delta^{11}\text{B}$ from the final chamber to the juvenile chambers, while B/Ca shows an opposing trend in the final whorl (Fig. 3). On average, from the final chamber to the f-7 chamber, Sr/Ca and Mg/Ca increase by $\sim 0.1 \mu\text{mol/mol}$ and $\sim 0.6 \text{ mmol/mol}$ respectively, while B/Ca decreases by $\sim 90 \mu\text{mol/mol}$ (Fig. 4). Chamber-averaged $\delta^{11}\text{B}$ across the entire dataset indicate a statistically significant increase from the final chamber to the f-7 chamber of $\sim 0.6 \text{ ‰}$.

3.3. $\delta^{13}\text{C}$ and ^{14}C age of WCO L4 samples

The ^{14}C ages of *C. lobatulus* at WCO L4 0–2 cm, 12–15 cm and 25–30 cm samples are 460 ± 45 , 505 ± 35 and 635 ± 40 years BP (before present; “present” refers to 1950 CE) respectively (Table S3). Atmospheric thermonuclear weapons testing after ~ 1950 CE artificially elevated the $^{14}\text{C}/\text{C}$ of the atmosphere, but “pre-bomb” estimates of Western European Continental shelf (WEC) surface water $^{14}\text{C}/\text{C}$ suggest a ^{14}C reservoir age of 480 ± 70 years BP (this assumes a well-mixed water column; see Table S4; Reimer and Reimer, 2001). Because these pre-bomb WEC ^{14}C reservoir age values are not statistically different from the core-top benthic foraminifera ^{14}C age, we use a ^{14}C reservoir age of 460 ± 45 years BP to estimate the calendar ages deeper in this

sediment core. Assuming the sedimentation rate at WCO L4 is consistent between each layer, the sedimentation rate can be calculated as the depth difference divided by the age difference between each pair of layers, yielding 0.28 cm/year between 0 and 13.5 cm, and 0.11 cm/year between 13.5 and 30 cm. The sediment core was collected in 2016 CE, the estimated calendar age of the 0–2 cm sample is therefore 2009–2016 CE, the 12–15 cm sample is 1953–1973 CE, and the 25–30 cm sample is 1814–1861 CE (Table S3).

These estimated ^{14}C ages agree with the constraints provided by the $\delta^{13}\text{C}$ results. The $\delta^{13}\text{C}$ values of *C. lobatulus* at WCO L4 0–2 cm, 12–15 cm, and 25–30 cm samples are 0.8 ‰ , 1.30 ‰ , and 1.29 ‰ respectively (Table 2, Fig. S5). Given the calendar ages assigned to this WEC sediment core, a 0.5 ‰ change in benthic foraminiferal $\delta^{13}\text{C}$ toward the present (from 12–15 cm and 25–30 cm to 0–2 cm) is consistent with a post-1970s CE appearance of the ‘ $\delta^{13}\text{C}$ Suess effect’ signal. This is consistent with benthic foraminiferal $\delta^{13}\text{C}$ records from the Northwest Atlantic shelf recording a post-1950s CE excursion of 0.45 ‰ (Mellon et al., 2019; Fig. S5).

3.4. Estimated BWT and pH from IFA data

The BWT at Site 999 at 9.28 ka estimated from the mean value of IFA Mg/Ca of *C. wuellerstorfi* (1.73 mmol/mol) is $3.5 \pm 0.6 \text{ }^\circ\text{C}$ (2SD), which is comparable to modern BWT in the Caribbean Sea ($\sim 3.85 \text{ }^\circ\text{C}$; Johnson and Purkey, 2009). Bottom water pH estimated from the mean value of

Table 1IFA results of Mg/Ca, B/Ca and $\delta^{11}\text{B}$ compare with values of bulk solution. *Cl* - *C. lobatulus*, *Cw* - *C. wuellerstorfi*^a.

		Range of spots	Range of mean values of tests ^b	Averaged intra-test variabilities (2SD) ^c	Mean values of populations (\pm 2SE) ^d	Inter-test variabilities (2SD) ^e	Solution (\pm 2SD)
Sr/Ca $\mu\text{mol}/\text{mol}$	<i>Cl</i> (CS_0–2)	0.88–2.19	1.18–1.69	0.18 \pm 0.25	1.42 \pm 0.06	0.26	1.42 \pm 0.11
	<i>Cl</i> (L4_0–2)	1.11–1.86	1.19–1.62	0.12 \pm 0.16	1.44 \pm 0.07	0.22	1.42 \pm 0.11
	<i>Cl</i> (L4_12–15)	1.04–2.14	1.09–1.90	0.16 \pm 0.20	1.35 \pm 0.12	0.41	1.37 \pm 0.11
	<i>Cl</i> (L4_25–30)	1.09–1.75	1.15–1.53	0.13 \pm 0.19	1.33 \pm 0.08	0.25	1.38 \pm 0.11
	<i>Cw</i> (Site 999)	1.14–1.84	1.22–1.66	0.11 \pm 0.13	1.39 \pm 0.08	0.28	1.28 \pm 0.10
Mg/Ca mmol/mol	<i>Cl</i> (CS_0–2)	1.71–6.96	1.89–6.39	0.91 \pm 1.18	2.92 \pm 0.50	2.07	3.37 \pm 0.17
	<i>Cl</i> (L4_0–2)	1.77–5.83	1.99–4.77	0.83 \pm 1.31	2.83 \pm 0.48	1.67	2.79 \pm 0.14
	<i>Cl</i> (L4_12–15)	1.67–3.88	1.91–3.44	0.49 \pm 0.59	2.28 \pm 0.22	0.76	2.42 \pm 0.12
	<i>Cl</i> (L4_25–30)	1.69–3.57	1.80–2.96	0.48 \pm 0.54	2.38 \pm 0.23	0.77	2.51 \pm 0.13
	<i>Cw</i> (Site 999)	0.93–2.95	1.40–2.15	0.58 \pm 0.50	1.73 \pm 0.14	0.46	1.76 \pm 0.09
B/Ca $\mu\text{mol}/\text{mol}$	<i>Cl</i> (CS_0–2)	197–423	230–346	57 \pm 51	299 \pm 19	77	265 \pm 24
	<i>Cl</i> (L4_0–2)	224–389	254–342	45 \pm 42	299 \pm 14	47	258 \pm 23
	<i>Cl</i> (L4_12–15)	218–429	256–415	42 \pm 37	313 \pm 27	94	266 \pm 24
	<i>Cl</i> (L4_25–30)	241–436	287–364	54 \pm 56	330 \pm 16	51	270 \pm 24
	<i>Cw</i> (Site 999)	137–374	206–287	57 \pm 54	239 \pm 14	45	229 \pm 21
$\delta^{11}\text{B}$ ‰	<i>Cl</i> (CS_0–2)	14.61–19.03	15.5–18.3	1.14 \pm 1.00	16.72 \pm 0.4	1.65	16.77 \pm 0.20
	<i>Cl</i> (L4_0–2)	14.52–19.16	15.3–17.7	1.59 \pm 1.08	16.22 \pm 0.38	1.31	16.14 \pm 0.27
	<i>Cl</i> (L4_12–15)	15.41–18.84	15.8–18.1	1.19 \pm 0.91	16.55 \pm 0.35	1.12	16.57 \pm 0.20
	<i>Cl</i> (L4_25–30)	15.56–19.03	16.3–17.9	1.14 \pm 0.84	17.04 \pm 0.22	0.78	ND
	<i>Cw</i> (Site 999)	15.35–17.83	16.2–17.1	0.92 \pm 0.70	16.71 \pm 0.18	0.61	16.66 \pm 0.25

^a See the explanation and specific calculation for the uncertainties (standard deviation and standard error) in section 2.4.2.

^b The mean values of tests are the average of spots within each individual foraminifer.

^c Intra-test variabilities were calculated within each foraminifer (2SD), then average the variabilities of each specimen to get a mean

^d The mean values of populations are the average of the mean values of tests.

^e Variabilities within the populations.

IFA $\delta^{11}\text{B}$ of *C. wuellerstorfi* (16.71 ‰) is 8.03 pH units, consistent with that estimated by Yu et al. (2010) who gave a pH of 8.02 ± 0.03 at 9.6 ka. Both values are slightly higher than the modern Caribbean Sea (\sim 7.9 pH units at a water depth of \sim 2800 m; Lauvset et al., 2024), which is consistent with a continuous decrease in pH in the Caribbean Sea since the Last Glacial Maximum (Yu et al., 2010).

The observed variability in seawater properties at WCO L4 (from 2008 to 2022 CE; McEvoy et al., 2023) temporally overlaps with the estimated age of our 0–2 cm sediment sample (2009–2016 CE). Observed temperatures at 50 m during this interval ranged from 7.65 to 16.39 °C, in agreement with Mg/Ca-estimated BWT values of 7.2 to 16.9 °C, narrowing to 8.2 to 15.1 °C when only the mean values of Mg/Ca of each test are considered (Fig. 5a). Similarly, the observed variation in seawater pH from 2009 to 2016 CE is 7.76 to 8.31 which is in good agreement with the estimate from IFA $\delta^{11}\text{B}$ which is 7.7 to 8.3, when only individual spots are considered, and 7.9 to 8.2 for whole test averages (Fig. 5b). A cross plot of BWT vs. pH further highlights the consistency between the observed seawater records and our IFA results (Fig. 5c).

The IFA estimated mean BWT values of populations of WCO 0–2 cm, 12–15 cm and 25–30 cm are: 10.6 ± 1.2 , 9.1 ± 0.7 , and 9.5 ± 0.8 °C (2SE; Table 2), respectively. The mean pH values of WCO 0–2 cm, 12–15 cm and 25–30 cm are 8.01 ± 0.04 , 8.07 ± 0.03 , 8.12 ± 0.03 (2SE; Table 2), respectively. The variabilities of both IFA estimated BWT and pH at 0–2 cm are higher than those within the other two deeper samples (Fig. 5; Table 2).

4. Discussion

4.1. Benthic foraminifera vital effect

The average intra-test and inter-test variabilities of Mg/Ca and B/Ca observed here (0.58 and 0.46 mmol/mol and 57 and 45 $\mu\text{mol}/\text{mol}$, respectively; Table 1) agrees well with values reported by Raitzsch et al. (2011) based on five specimens of *C. wuellerstorfi* core-top samples from the South Atlantic. The trends and range of variability of Mg/Ca and B/Ca within the final whorl (Figs. 3, 4) are also consistent with Raitzsch et al. (2011). In contrast, intra- and inter-test variabilities of $\delta^{11}\text{B}$ observed in this study (0.92 ‰ and 0.61 ‰; 2SD) are lower than those in Raitzsch et al. (2020; 1.3 ‰ and 1.62 ‰; 2SD). We attribute this primarily to differences in analytical strategy and sampling design. Recent instrumental and methodological developments enable robust $\delta^{11}\text{B}$ measurements from smaller ablated areas and shorter analysis times (Standish et al., 2025), which in turn allow us to perform systematic chamber-by-chamber analyses on specimens with 250–355 μm size fraction. In contrast, Raitzsch et al. (2020) analysed large craters (\geq 300 μm) to get quasi-bulk values for a single test (350–400 μm size fraction). Although the internal precision of individual ablation spots (\sim 1 ‰, 2SE) and the long-term reproducibility of reference materials (\sim 1.3 ‰, 2SD) are comparable to Raitzsch et al. (2020), our increased number of spatially resolved analyses per test provides stronger statistical constraints on intra-shell $\delta^{11}\text{B}$ variability. Besides, differences in the protocols adopted here (data reduction combined with chemical cleaning)

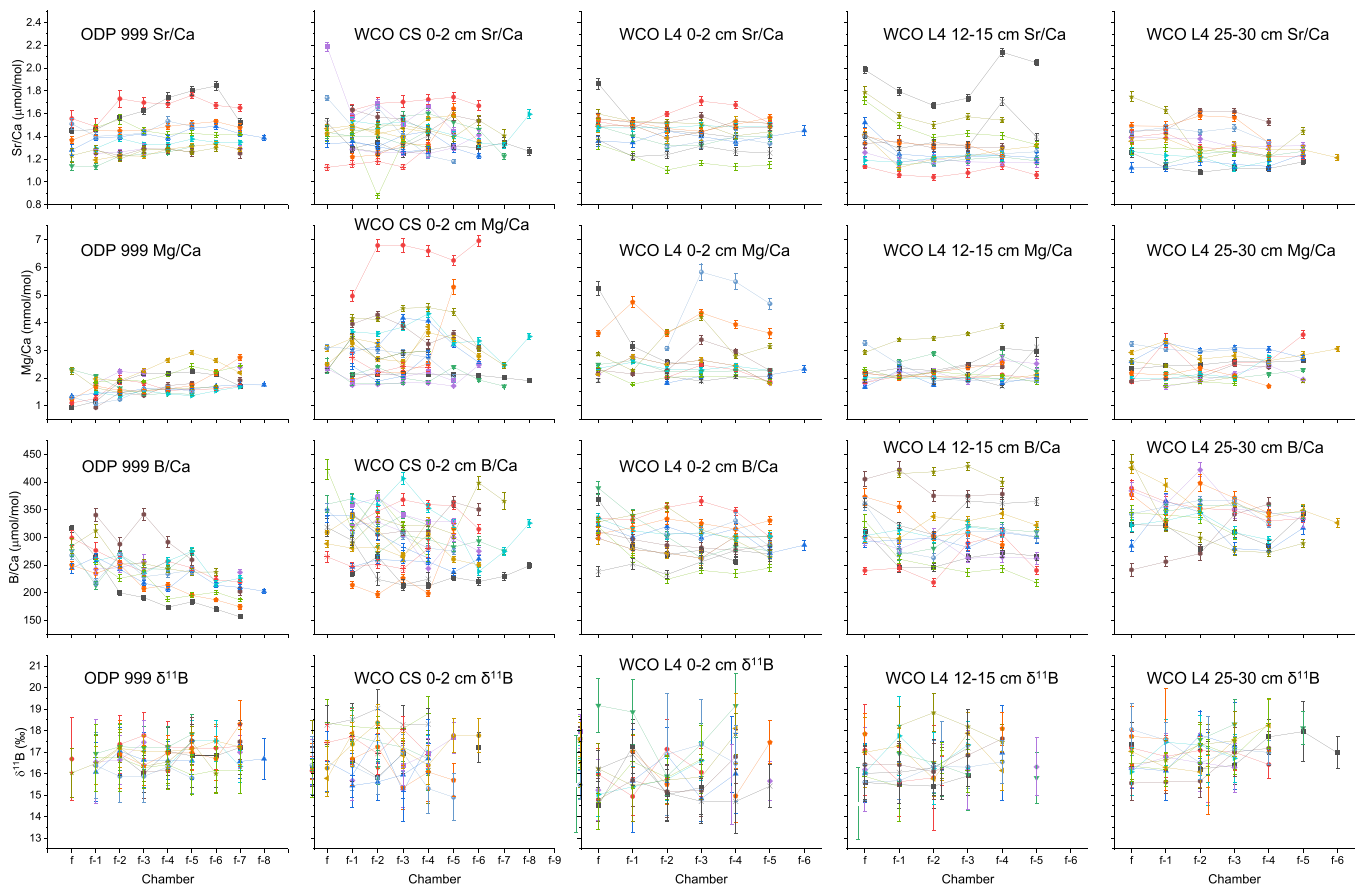


Fig. 3. Intra-test variabilities of Sr/Ca, Mg/Ca, B/Ca, and $\delta^{11}\text{B}$. f represents the final chamber, f-1 is the penultimate one, and so on. Each individual is represented by symbols and lines with different shapes and colours, error bars represent $\pm 2\text{SE}$.

compared to those used by Raitzsch et al. (2020) (data reduction only), aimed at minimizing potential contamination, may also contribute to the lower variability observed in this study (see SI2 for details). Despite these differences, the distribution of $\delta^{11}\text{B}$ values in the final whorl observed here broadly agrees with two large specimens ($\sim 600\ \mu\text{m}$) analysed in Raitzsch et al. (2020). The one specimen of *C. wuellerstorfi* from Sadekov et al. (2019), however, shows a larger within whorl change than any of the 12 specimens we analysed at ODP 999 (Fig. S6).

The elemental and isotopic composition of foraminiferal calcite is controlled by both the environment experienced during life and biologically related processes often grouped together into the term ‘vital effects’ (de Nooijer et al., 2014). In situ analysis of foraminifera offers a tool to elucidate the relative roles of ambient seawater chemistry and vital effects on the geochemical spatial heterogeneity observed within an individual shell (Fehrenbacher et al., 2024). Significant intra-test trends of Sr/Ca, Mg/Ca, B/Ca and $\delta^{11}\text{B}$ were found within *C. wuellerstorfi* from ODP Site 999 (Figs. 3, 4). The broad agreement with previous studies of this kind (e.g. Raitzsch et al., 2020) lends support for our use of our ODP 999 to further explore cause of these trends in *C. wuellerstorfi*, with possible reasons including: i) bottom-water environmental variability; ii) microhabitat environmental variability in the sediment-water interface during growth; iii) ontogenetic changes in physiology (e.g. respiration and calcification rate) during the foraminiferal life cycle. Bottom water environmental variation at ODP 999 can be largely excluded since a variation of 0.4 mmol/mol of Mg/Ca equates to a difference of more than 1 °C of bottom water temperature (Healey et al., 2008), and 0.6 ‰ variation of $\delta^{11}\text{B}$ transfers to bottom water pH is ~ 0.1 pH units. Instrumental observations from ~ 1310 m water depth in the Caribbean Sea (the deepest in this region that is available) indicate sub-annual changes of temperature of ~ 0.01 °C, and pH of ~ 0.01 pH

units (Muller-Karger et al., 2013). It is reasonable to expect the sub-annual changes at ODP 999 with water depth of 2828 m, are smaller, which therefore cannot explain the observed intra-test variation of Mg/Ca and $\delta^{11}\text{B}$ of *C. wuellerstorfi*. Microhabitat-related porewater effects can also be discounted because *C. wuellerstorfi* is a strict epifaunal species that resides above the sediment-water interface, and proxies such as B/Ca, $\delta^{11}\text{B}$, and $\delta^{13}\text{C}$ are largely insensitive to porewater chemistry (Lutze and Thiel, 1989; Rae et al., 2011; Schmittner et al., 2017). We therefore propose that the intra-test variation of *C. wuellerstorfi* predominantly reflects ontogenetic effects, particularly changes in metabolic activity and calcification rate as the foraminifera grow through their life cycle (Hohenegger, 2018; Schmiedl et al., 2004).

The intra-test patterns observed here indicates that during the growth of foraminifera, as metabolic activity and calcification rate decrease (Hohenegger, 2018; Schmiedl et al., 2004), test Mg/Ca, Sr/Ca, and $\delta^{11}\text{B}$ decrease while B/Ca increases (Fig. 4). In addition, we also document significant variability between individuals in a population (Table 1). Again, the relatively stable deep-sea environment at ODP 999 argues against this variability being the result of environmental changes. To further examine the influences of individual variations in respiration rate and calcification rate, we additionally examined the variation in whole test composition with test weight, test area (projected area; see ‘Methods’), and test area-density (ratio of foraminiferal weight to its area; Fig. 6). Assuming broadly comparable lifespans among adult individuals, test weight, test area, and area-density can be used as first-order, relative proxies for several physiological processes integrated over the life cycle. Specifically, test weight represents cumulative calcification, and area-density represents calcification intensity (Marshall et al., 2013), whereas test area provides a measure of test size, which has been shown to scale with respiration rate in adult

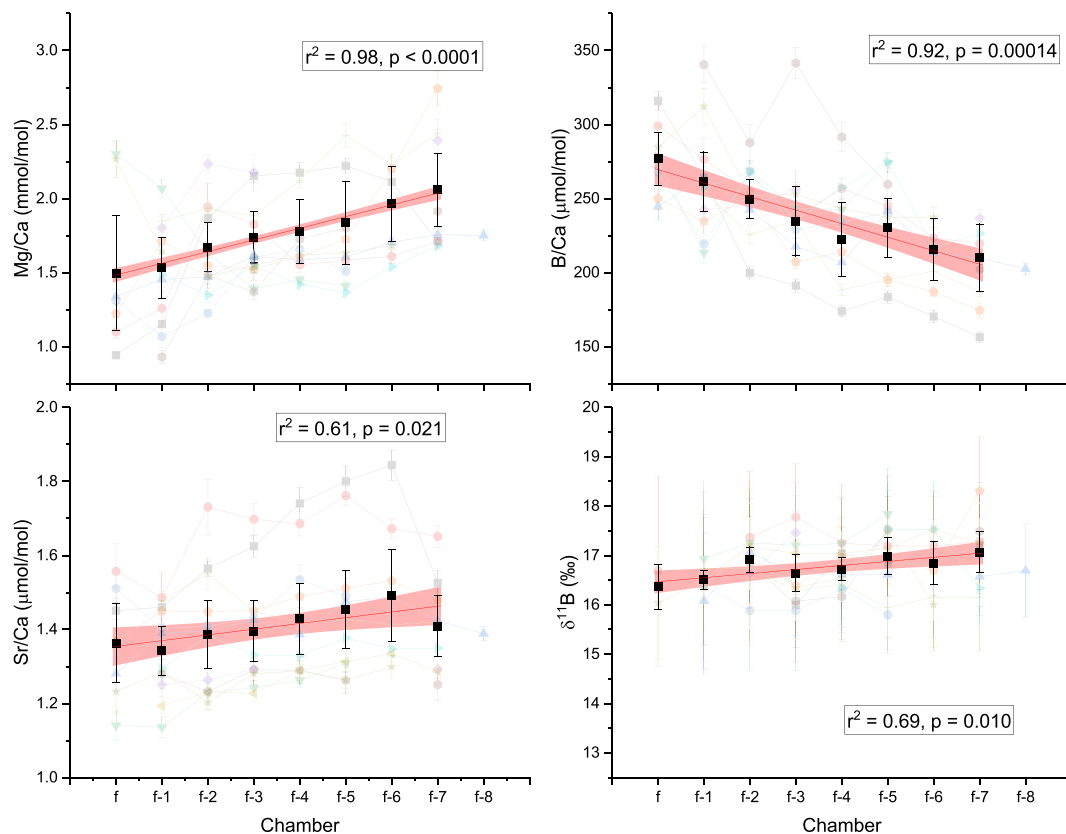


Fig. 4. Intra-test variabilities of Sr/Ca, Mg/Ca, B/Ca, and $\delta^{11}\text{B}$ within *C. wuellerstorfi* from ODP Site 999. f represents the final chamber, f-1 is the penultimate one, and so on. Black squares represent averaged values of each chamber. Red lines with shaded bands represent linear fits with 95% confidence intervals of the regression, which do not include the analytical uncertainties of individual data points. Error bars represent $\pm 2\text{SE}$ of individual measurements. (For interpretation of the references to colour in this figure legend, the reader is referred to the web version of this article.)

Table 2

Summary of the chronological framework and reconstructed test-averaged temperature and pH at WCO L4.

Core depth	Calendar Age	$\delta^{13}\text{C}$	Reconstructed T ($\pm 2\text{SE} / 2\text{SD}$)	Reconstructed pH ($\pm 2\text{SE} / 2\text{SD}$)
cm	CE	‰	°C	pH units
0–2	2009–2016	0.80	$10.6 \pm 1.2 / 4.5$	$8.01 \pm 0.04 / 0.14$
12–15	1953–1973	1.30	$9.1 \pm 0.7 / 2.5$	$8.07 \pm 0.03 / 0.12$
25–30	1814–1861	1.29	$9.5 \pm 0.8 / 2.7$	$8.12 \pm 0.03 / 0.10$

foraminifera (Burke et al., 2025). Positive relationships among area, weight, and area-density suggest coupling between respiration and calcification at the individual level, such that larger individuals tend to exhibit higher rates of respiration and calcification over their lifetime (Fig. S7). At the level of an individual, metabolic activity and calcification rate of foraminifera decrease with age as foraminifera approach a late growth stage (Hohenegger, 2018; Schmiedl et al., 2004); whereas at the level of the population, adult individuals with smaller test sizes reflect lower average growth rates over their lifetime. Statistically significant negative relationships are observed between B/Ca and both weight and area-density ($p < 0.05$; Fig. 6). In contrast, Sr/Ca shows weak positive trends with test weight and area, and Mg/Ca shows a weak positive trend with area-density, although these relationships are not statistically significant ($0.05 < p < 0.1$; Fig. 6). Overall, the inter-test relationships are broadly consistent with the trends observed within individual tests, suggesting lower respiration or calcification rates (whether at the population scale or as an individual ages) are associated with decreasing Mg/Ca, Sr/Ca, and increasing B/Ca (Figs. 4, 6).

The mechanisms of foraminiferal chemical and isotopic composition variation during ontogeny and between individuals are complex and

may be related to: i) Trace element and isotope partition coefficient variation with changes of calcite precipitation rate (e.g. Dissard et al., 2010; Holland et al., 2017; Salmon et al., 2016); ii) Variations in rates of ion transport control across membranes into the calcifying space (e.g., Zeebe et al., 2003); and iii) Variations in CO_2 diffusion and/or $\text{B}(\text{OH})_3$ diffusion toward the site of calcification (e.g. de Nooijer et al., 2009; François et al., 2025; Gagnon et al., 2021). An additional complication should also be noted that when results from inorganic precipitation experiments are invoked to interpret rate-related effects in biogenic calcification, direct quantification of instantaneous calcification rates is difficult, because foraminiferal calcification is episodic and growth surface areas are hard to quantify. Nevertheless, recent modelling work estimates the instantaneous calcification rates of *C. wuellerstorfi* or *C. mundulus* are ~ 0.5 to $1.5 \times 10^{-6} \text{ mol/m}^2/\text{s}$ (Jia et al., 2024), which overlap with precipitation rates commonly used in typical inorganic calcite experiments (e.g. Mavromatis et al., 2013; Noireaux et al., 2015). Nonetheless, until the actual rates of calcification in foraminifera are better quantified, we use such comparisons here only to provide context rather than to imply mechanistic equivalence.

With these limitations in mind, the positive relationship between Sr partition coefficients D_{Sr} and foraminiferal growth rate has also been reported in planktic foraminifera (e.g. Holland et al., 2017; Kisakürek et al., 2008), and other species of benthic foraminifera (e.g. Dissard et al., 2010; Dueñas-Bohórquez et al., 2011) and is also consistent with many inorganic precipitation experiments showing increasing D_{Sr} with precipitation rate (e.g. Lorens, 1981; Tang et al., 2008; Tesoriero and Pankow, 1996). This provides a plausible explanation for higher Sr/Ca at higher calcification rates, although Rayleigh fractionation in a partially isolated calcifying fluid could produce similar trends as a function of precipitation rate (Elderfield et al., 1996). D_{Mg} in inorganic

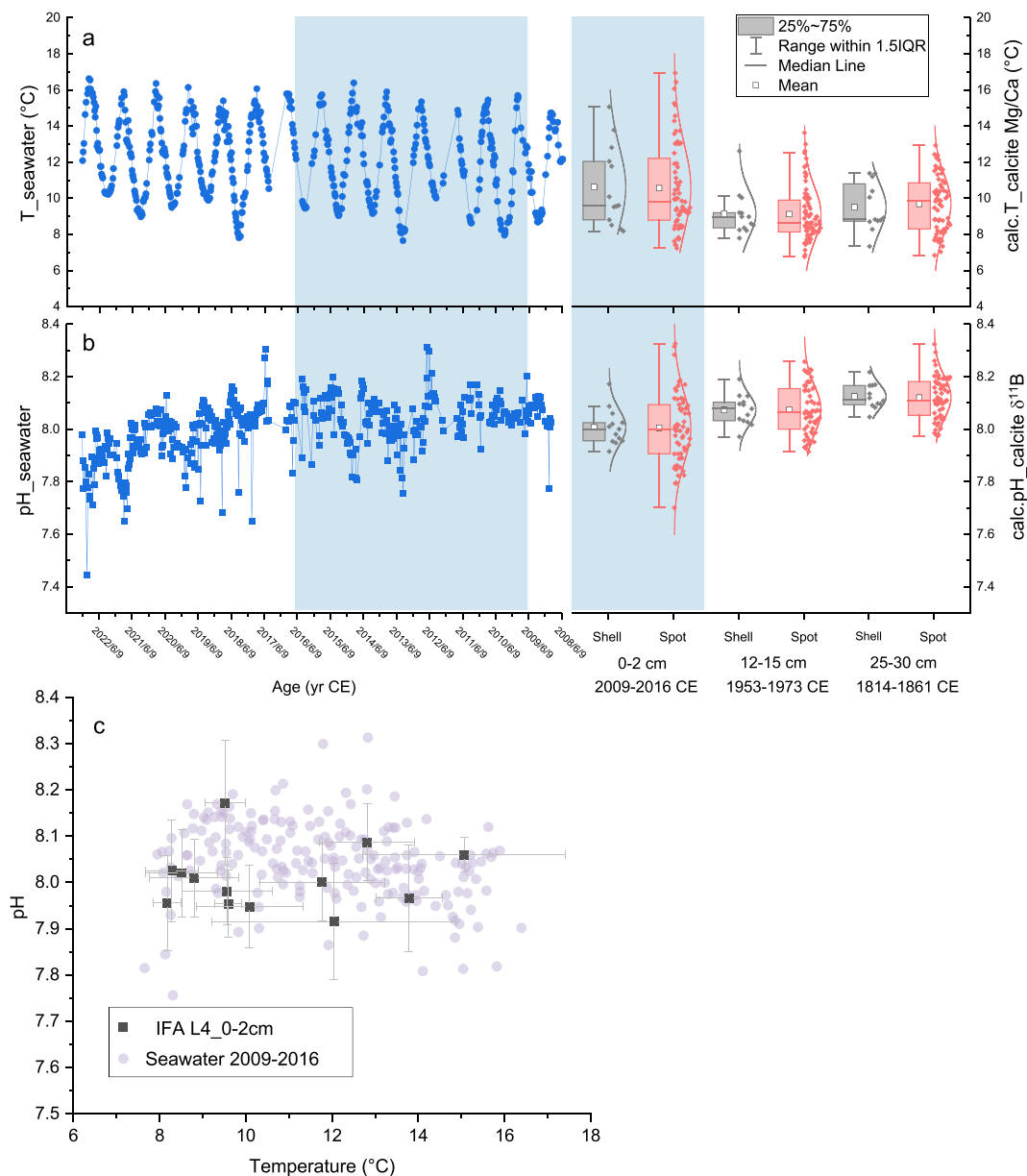


Fig. 5. Comparison between instrumental observations of the water column and IFA-derived estimates of bottom water temperature (BWT) and seawater pH from *C. lobatulus* at WCO Site L4. a. Instrumental temperature record at WCO Site L4 (depth = 50 m; McEvoy et al., 2023) compared with IFA-derived seawater temperature estimates, b. Instrumental pH record at WCO Site L4 (depth = 50 m; McEvoy et al., 2023) compared with IFA-derived seawater pH estimates, c. Cross-plots of temperature versus pH comparing instrumental seawater observations (2009–2016) with IFA-derived estimates from the 0–2 cm sediment interval only. In panels (a) and (b), grey boxes and symbols represent test-averaged values, while red boxes and symbols represent means of time-resolved spot measurements. Blue bands highlight the 2009–2016 CE time-series records, which were compared to 0–2 cm sediment sample. In panel (c), error bars represent $\pm 2\text{SE}$. (For interpretation of the references to colour in this figure legend, the reader is referred to the web version of this article.)

precipitation is also sensitive to precipitation rates, however, both positive (Mavromatis et al., 2013) and negative relationships (e.g. Gabitov et al., 2014; Mucci and Morse, 1983) have been observed under different experimental settings. Besides, the one to two orders of magnitude lower Mg/Ca ratio in the most hyaline species compared to inorganic carbonate indicates that the incorporation of Mg into foraminifera is strongly affected by biological processes (e.g. Bentov and Erez, 2006; de Nooijer et al., 2014). The positive relationship between Mg/Ca and growth rate within low-Mg foraminifera observed in this study and previous studies (e.g. Dissard et al., 2010; Dueñas-Bohórquez et al., 2011; Holland et al., 2017), may therefore reflect faster calcification and/or restriction in discrimination against Mg^{2+} in younger or faster-growing individuals.

Similar to D_{Sr} , inorganic precipitation experiments show that the

boron partition coefficient (D_{B}) generally increases with precipitation rate (e.g., Gabitov et al., 2014; Mavromatis et al., 2015; Uchikawa et al., 2015), whereas $\delta^{11}\text{B}$ remains relatively constant as rate changes (e.g., Noireaux et al., 2015). In contrast to the Sr/Ca patterns, the opposite intra- and inter-test patterns of B/Ca observed indicate that other factors than precipitation rate dominate B incorporation (Figs. 4, 6). The decoupling between B/Ca and $\delta^{11}\text{B}$ patterns at the intra-test scale (Fig. 4) indicates that neither the diffusive boundary layer (DBL) pH nor calcifying fluid pH alone can account for the observed patterns, as this mechanism would predict covariation between B/Ca and $\delta^{11}\text{B}$. Decoupled carbonate chemistry experiments on incubated benthic foraminifera (Coenen et al., 2024; Kaczmarek et al., 2015), and planktic foraminifera (Howes et al., 2017) demonstrate that B/Ca is primarily regulated by the relative availability of $\text{B}(\text{OH})_4^-$ versus dissolved

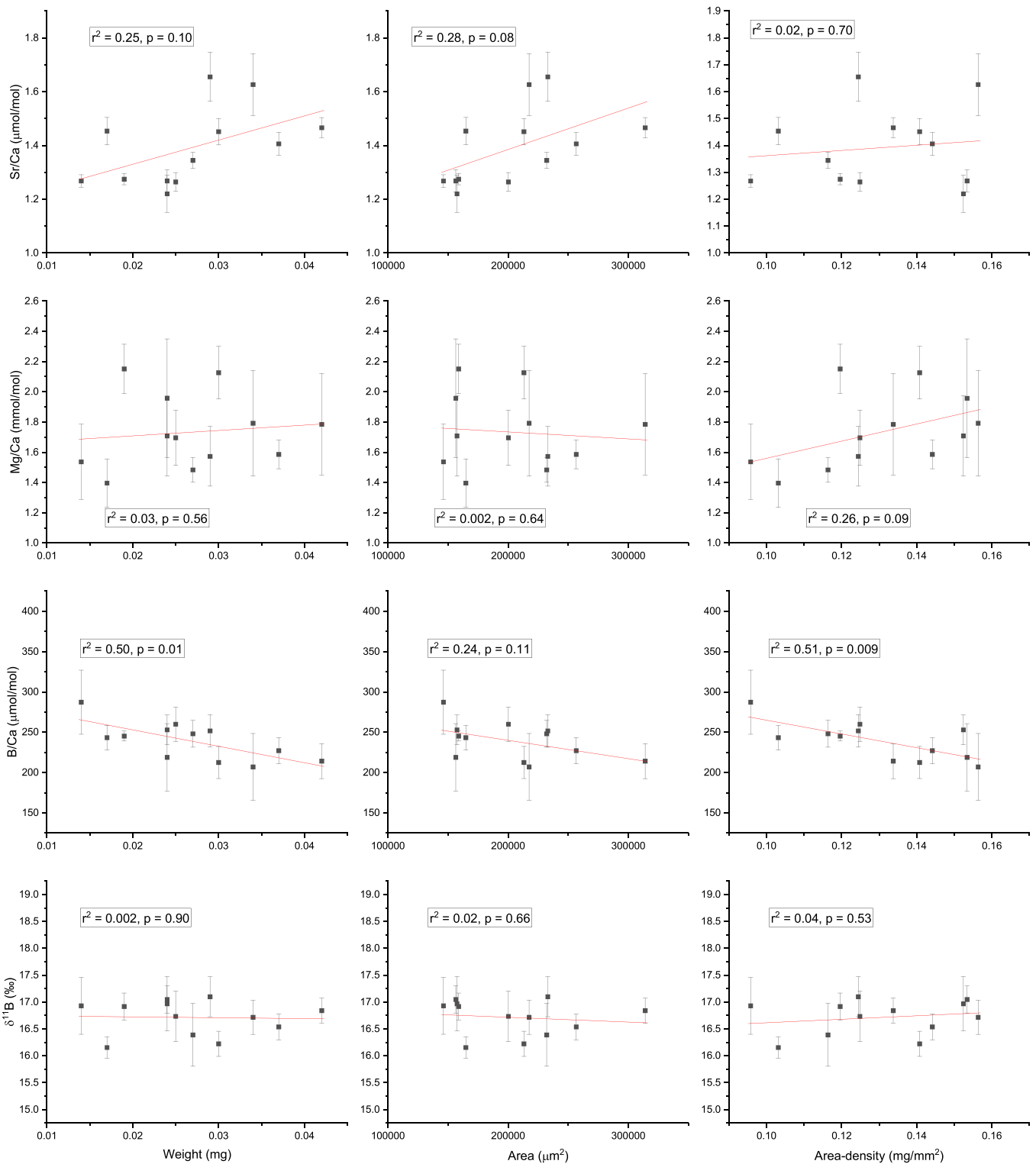


Fig. 6. Inter-test variabilities of *C. wuellerstorfi* Mg/Ca, B/Ca and $\delta^{11}\text{B}$ from ODP 999. Test-averaged values of Mg/Ca, B/Ca and $\delta^{11}\text{B}$ of each individual versus test weight, silhouette area, and area-density. Red line represent linear fitted lines, error bars represent $\pm 2\text{SE}$. (For interpretation of the references to colour in this figure legend, the reader is referred to the web version of this article.)

inorganic carbon (DIC), consistent with competition between boron and carbon species for lattice incorporation. Within this framework, variations in metabolic activity during ontogeny may modify the composition of calcifying fluid in *C. wuellerstorfi*, especially HCO_3^- supply and DIC turnover associated with ion transport and respiration (e.g. de Nooijer et al., 2014; Toyofuku et al., 2017). In contrast, $\delta^{11}\text{B}$ in *C. wuellerstorfi*

shows limited variation attributable to ontogeny and/or vital effects. Although a gradual and statistically significant decrease of $\sim 0.6\text{‰}$ is observed along the final whorl from the f-7 to f chamber (Fig. 4), no systematic relationships are detected between $\delta^{11}\text{B}$ and test weight, size, or area density at the individual level (Fig. 6). These results indicate that, while subtle ontogenetic influences cannot be excluded, $\delta^{11}\text{B}$

appears comparatively insensitive to first-order physiological effects, supporting its robustness as a recorder of ambient seawater pH, consistent with observations from core-top studies (e.g., Rae et al., 2011). The modest intra-test decrease observed along the final whorl is directionally consistent with diffusion–reaction model predictions for DBL effects in symbiont-barren species (Zeebe et al., 2003), which suggest decreasing $\delta^{11}\text{B}$ with increasing test radius (Zeebe et al., 2003), and for *C. wuellerstorfi* this effect may be amplified because chamber size increases rapidly along the final whorl (Holbourn et al., 2013). However, the lack of such a signature at the individual level (e.g. Fig. 6) may indicate other factors are at play. Spatial heterogeneity within the foraminiferal test may also contribute to the observed decoupling between B/Ca and $\delta^{11}\text{B}$. Variations in crystal structure, organic matrix distribution, or microstructural domains across chambers may influence boron partitioning into calcite without proportionally modifying isotopic composition (Bentov and Erez, 2006; Branson et al., 2015; de Nooijer et al., 2014). Such heterogeneity may lead to localized enrichment or depletion in B/Ca while $\delta^{11}\text{B}$ remains comparatively stable, particularly if isotopic signatures are fixed early during calcification (Rollion-Bard et al., 2003; Gagnon et al., 2021). This type of micro-scale variability likely represents an additional, and currently underexplored, control on boron systematics in foraminifera, although the spatial resolution necessary to directly detect potential $\delta^{11}\text{B}$ banding within individual foraminiferal chambers remains beyond the capability of current in situ analytical methods.

Regardless of the causes of the inter- and intra-test variations we observe here, from the perspective of IFA applications, the observed intra-test variability suggests multiple chambers should be analysed to get whole-test average values and, if multiple chambers are analysed, the same chambers (e.g., analyse f-1 to f-6 chambers of all the specimens) should be targeted consistently to minimise any biases arising from ontogenetic effects. Based on the inter-test variabilities we observed, a narrow range of test sizes should be chosen in future work, or if a range is used, some attempt to normalise the influence of test size should be carried out. It is also likely that the trends observed in *C. wuellerstorfi* at ODP 999, and the related discussions, are largely species-specific, and one should be cautious when extending our findings to other species.

4.2. Application of individual benthic foraminiferal analysis

The consistency between IFA generated BWT and pH with observed seawater values at ODP Site 999 and the 0–2 cm samples from WCO L4 provides a strong ground-truthing for the IFA methodology and support its use in generating palaeo-records (Fig. 5). Before interpreting the IFA records from WCO L4 sediment core, the sources of the inter- and intra-variation we observe at this site should be considered. Given the close phylogenetic relationship between *C. wuellerstorfi* and *C. lobatulus* (Schweizer et al., 2009), the ontogenetic and inter-individual patterns observed in *C. wuellerstorfi* from ODP 999, which is characterized by minimal environmental annual variability (Gallegos, 1996), were used as a methodological reference to isolate the relative contributions of vital effects from variations in Mg/Ca and $\delta^{11}\text{B}$ of *C. lobatulus* specimens from WCO stations caused by the more extreme environmental seasonality that occurs at the English Channel site (Fig. 5, Fig. S2; McEvoy et al., 2023). At ODP 999, $\delta^{11}\text{B}$ shows no systematic ontogenetic dependence at the inter-test level (Fig. 6), indicating that test-averaged values largely remove any intra-test trends (Fig. 4). The remaining inter-test variability (0.61 ‰, 2SD; Table 1) at ODP 999 therefore represents a reasonable upper limit for variability caused by individual and analytical uncertainty. At WCO L4, $\delta^{11}\text{B}$ variabilities substantially exceed this limit, requiring the contribution from seasonal variability. For the WCO L4 0–2 cm interval, the inter-test variability is 1.31 ‰ (2SD), implying a minimum seasonal contribution of 1.16 ‰ ($\sqrt{1.31^2 - 0.61^2}$), equivalent to a pH change of ~ 0.15 pH units, which is very consistent with the

variability of instrumental records of pH at L4 from 2009 to 2016 (0.17 units; 2SD; McEvoy et al., 2023). For Mg/Ca, at the inter-test level, the results at ODP 999 show a weak dependence on test area-density (Fig. 6; $p = 0.09$). The area-density of *C. lobatulus* at WCO L4 is however tightly clustered (~ 0.09 – 0.12) and when projecting this range onto the ODP Mg/Ca vs. area-density relationship the expected vital effects contribution is small (~ 0.2 mmol/mol), far below the observed inter-test variabilities at WCO L4 (0.76–1.67 mmol/mol; Table 1). Considering the full inter-test variability at ODP 999 (0.46 mmol/mol, 2SD; Table 1) as the upper bound vital effects plus analytical uncertainty, at the L4 0–2 cm interval, the observed ± 1.67 mmol/mol inter-test variability (2SD; Table 1) still requires an additional contribution of at least ± 1.61 mmol/mol ($\sqrt{1.67^2 - 0.46^2}$). These results demonstrate that the enhanced inter-test observed at WCO L4 cannot be explained by vital effects alone. Instead, seasonal environmental variability appears to dominate the Mg/Ca and $\delta^{11}\text{B}$ variabilities recorded by individual foraminiferal tests at this site.

Based on whole-test averages, 1814–1861 CE (25–30 cm layer) is 0.4 °C warmer than 1953–1973 CE (12–15 cm layer) (Fig. 5a; Table 2), which can be related to a local Northern Hemisphere temperature decline in 1945 CE and around 1970 CE (Thompson et al., 2010), and a cooling of ~ 0.5 °C during the 1960s to 1980s has also been observed in WCO E1, an adjacent long-term instrumental time-series station (McEvoy et al., 2023; see Fig. S1 for location). Our foraminiferal-Mg/Ca based record then indicates a 1.5 °C warming of seawater at WCO L4 after the 1950s to recent, corresponding to a warming rate of ~ 0.03 °C/yr (Fig. 5a), which is in excellent agreement with warming inferred from instrumental water-column records at WCO L4 from 1986 to 2021 (~ 0.03 °C/yr; McEvoy et al., 2023), as well as the overall warming trend of sea surface temperatures across the north-west European Shelf (~ 0.03 °C/yr over the last 40 years; Cornes et al., 2023). Warming rates across the north-west European Shelf are highly spatially heterogeneous, showing a pronounced east-west contrast (Cornes et al., 2023). The strongest warming occurs in the eastern shelf seas (e.g. the North Sea), where seawater temperatures are dominated by atmospheric forcing, whereas weaker warming is observed toward the western regions that are more influenced by North Atlantic waters (Cornes et al., 2023). The WCO L4 station, located in the middle, reflects the combined influences of both these regimes.

Our test-averaged $\delta^{11}\text{B}$ data suggest that from the mid-19th century CE to recent, seawater pH in the Western Channel declined by 0.11 pH units (Fig. 5b; Table 2). This trend is in good agreement with the modelled evolution of annual-global surface ocean pH driven by anthropogenic CO₂ uptake (Jiang et al., 2019; Fig. 7). Instrumental observations from the Western English Channel (Findlay et al., 2025; Ostle et al., 2016), and open ocean sites, e.g., Bermuda Atlantic Time-series (BATS; Bates and Johnson, 2020), also indicate the decline of seawater pH for the last ~ 40 years (Fig. 7). Compared with BATS, the seawater pH or the carbonate system from the Western English Channel and the North Sea not only exhibit significant seasonal variation, but also exhibit much larger interannual variability as shown by the annual mean (Fig. 7). Such enhanced high-frequency variability at the Western English Channel reflects the combined influences of local and seasonal processes, including temperature-dependent carbonate chemistry, biological activities like production and respiration, freshwater and alkalinity inputs, and tidal dynamics and mixing (Carstensen and Duarte, 2019; Findlay et al., 2025; Sims et al., 2022; Worrall et al., 2016; Fig. S2). Although instrumental pH records from the UK coast exhibit substantially large interannual variability, this variability is superimposed on a long-term decline which is consistent with the trends observed at the open ocean (e.g., BATS) and in modelled globally annually average seawater pH (Fig. 7). As highlighted by Carstensen and Duarte (2019), such high-frequency variability implies that the estimate of acidification rate in coastal environments is sensitive to the chosen or available time window. Nevertheless, the consistency of the underlying

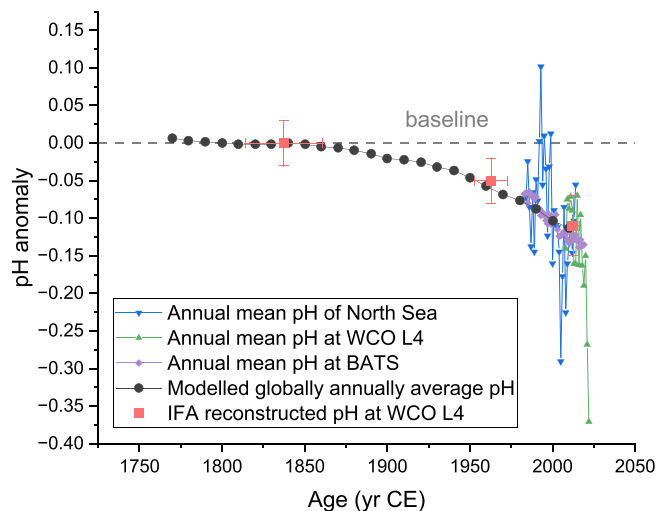


Fig. 7. Comparison of IFA-reconstructed pH anomaly records at WCO L4 with instrumental- and model-based pH anomalies over the past 150 years. The latter include model-based annually averaged global surface ocean pH anomalies (Jiang et al., 2019), observation-based annual mean pH anomalies from UK coastal regions in North Sea (Ostle et al., 2016) and WCO L4 (McEvoy et al., 2023), and open-ocean site BATS (Bates and Johnson, 2020). Red squares represent IFA-reconstructed pH anomalies at WCO L4. Vertical error bars indicate $\pm 2SE$ of the population mean pH estimates derived from IFA, while horizontal error bars represent the age uncertainty associated with each sediment interval. The grey dashed line represents the baseline, set to 8.17 pH units for the North Sea, L4, and the modelled record, 8.19 for BATS, and 8.12 for IFA, to align the records. (For interpretation of the references to colour in this figure legend, the reader is referred to the web version of this article.)

trends across UK coastal, open-ocean and modelled records explains the good agreement between the test-averaged IFA pH reconstructions and the modelled evolution of annual-global surface ocean pH, despite the involvement of complicated local processes in coastal environments (Fig. 7).

In terms of seasonal variability, cross plots of pH and BWT generated by our IFA method agree well with the observed seasonal variation (Fig. 5c), supporting its use to reconstruct the average seasonal range in BWT and pH beyond the observation record. The IFA Mg/Ca and $\delta^{11}B$ are more variable for 0–2 cm samples (with an age of 2009–2016) than the two older sediment layers (1953–1973 and 1814–1861) examined, which implies that from pre-industrial to recent, the seasonal variability of seawater temperature and pH has increased (Fig. 5a, b). Although our temporal sample set is small, increased seasonal amplitude of seawater conditions has been reported in the Mediterranean Sea (Pisano et al., 2020) and the subtropical North Atlantic (Bates and Johnson, 2020). Furthermore, modelling of future intra-annual variability in sea surface temperature of high latitude northern hemisphere regions under RCP 8.5 and 4.5 scenarios also exhibits an increasing trend (Ruela et al., 2020). As for the amplitude of seasonal cycles of pH, modelling work indicates a decreasing trend at the global scale but with regional variabilities (Kwiatkowski and Orr, 2018), with some high latitude regions exhibiting increasing amplitudes like those observed here.

5. Conclusion

By combining physical and chemical cleaning protocols with strict data screening strategies for time-resolved data, we effectively reduced the influence of contamination and generated comparable results for multi-test means with bulk solution values for a variety of El/Ca ratios and for $\delta^{11}B$. For *C. wuellerstorfi* at ODP Site 999, the uncertainties on the average of 12 individuals by IFA are also comparable in precision to solution methods being as low as 0.14 mmol/mol and 0.18 ‰ (2SE) for Mg/Ca and $\delta^{11}B$, respectively. The observed intra-test variabilities,

together with the significant inter-test relationships for B/Ca, indicate a major influence from ontogeny-related vital effects on Sr/Ca, Mg/Ca, and B/Ca in *C. wuellerstorfi*, with minor intra-test variations (0.6 ‰) from the f to f-7 chamber for $\delta^{11}B$, but with no significant inter-test trends. Applying our improved multi-proxy IFA method to a core from the English Channel with large seasonal variability, we show that IFA Mg/Ca and $\delta^{11}B$ are reliably able to recover seasonal-scale climate information. A preliminary down-core study from this site also reveals the warming and acidification of the English Western Channel from pre-industrial to recent. These results are consistent with direct water-column observations and show that IFA methodologies open up a new window into seasonal-scale carbon cycle variations in the recent and more distant past.

Supplementary data to this article can be found online at <https://doi.org/10.1016/j.chemgeo.2026.123395>.

CRediT authorship contribution statement

Zifei Yang: Writing – review & editing, Writing – original draft, Methodology, Investigation, Formal analysis, Data curation, Conceptualization. **Christopher D. Standish:** Writing – review & editing, Methodology, Investigation, Data curation. **Rachel M. Brown:** Investigation, Data curation. **Patrick A. Rafter:** Writing – review & editing, Investigation, Data curation. **Malcolm B. Hart:** Writing – review & editing, Resources. **Tali L. Babila:** Writing – review & editing, Supervision, Methodology, Funding acquisition, Conceptualization. **Gavin L. Foster:** Writing – review & editing, Supervision, Resources, Methodology, Funding acquisition, Conceptualization.

Declaration of competing interest

The authors declare that they have no known competing financial interests or personal relationships that could have appeared to influence the work reported in this paper.

Acknowledgements

Samples used in this research were provided by the Western Channel Observatory, and the Ocean Drilling Program. This work was funded by Natural Environment Research Council grant NE/W009625/1 to G.L.F. and T.L.B. We thank Andy Milton and Megan Wilding for analytical support.

Data availability

Data are available through Figshare at <https://doi.org/10.6084/m9.figshare.30565613>.

References

- Altman, D.G., Bland, J.M., 2005. Standard deviations and standard errors. *BMJ* 331, 903.
- Babila, T.L., Penman, D.E., Standish, C.D., Doubrava, M., Bralower, T.J., Robinson, M. M., Self-Trail, J.M., Speijer, R.P., Stassen, P., Foster, G.L., Zachos, J.C., 2022. Surface ocean warming and acidification driven by rapid carbon release precedes Paleocene-Eocene Thermal Maximum. *Sci. Adv.* 8 eabg1025.
- Barker, S., Greaves, M., Elderfield, H., 2003. A study of cleaning procedures used for foraminiferal Mg/Ca paleothermometry. *Geochem. Geophys. Geosyst.* 4, 1–20.
- Bates, N.R., Johnson, R.J., 2020. Acceleration of ocean warming, salinification, deoxygenation and acidification in the surface subtropical North Atlantic Ocean. *Commun. Earth Environ.* 1, 33.
- Bentov, S., Erez, J., 2006. Impact of biomineralization processes on the Mg content of foraminiferal shells: A biological perspective. *Geochem. Geophys. Geosyst.* 7.
- Branson, O., de Nooijer, L.J., 2025. Calcium Carbonate Biomineralisation: Insights from Trace elements. *Elements* 21, 105–111.
- Branson, O., Kaczmarek, K., Redfern, S.A.T., Misra, S., Langer, G., Tylliszczak, T., Bijma, J., Elderfield, H., 2015. The coordination and distribution of B in foraminiferal calcite. *Earth Planet. Sci. Lett.* 416, 67–72.
- Burke, J.E., Elder, L.E., Maas, A.E., Gaskell, D.E., Clark, E.G., Hsiang, A.Y., Foster, G.L., Hull, P.M., 2025. Physiological and morphological scaling enables gigantism in pelagic protists. *Limnol. Oceanogr.* 70, 461–476.

- Carstensen, J., Duarte, C.M., 2019. Drivers of pH Variability in Coastal Ecosystems. *Environ. Sci. Technol.* 53, 4020–4029.
- Chalk, T.B., Foster, G.L., Wilson, P.A., 2019. Dynamic storage of glacial CO₂ in the Atlantic Ocean revealed by boron [CO₃²⁻] and pH records. *Earth Planet. Sci. Lett.* 510, 1–11.
- Coenen, D., Evans, D., Hauzer, H., Nambiar, R., Jurikova, H., Dumont, M., Kanna, P., Rae, J., Erez, J., Cotton, L., Renema, W., Müller, W., 2024. Boron isotope pH calibration of a shallow dwelling benthic nummulitid foraminifera. *Geochim. Cosmochim. Acta* 378, 217–233.
- Cornes, R., Tinker, J., Hermanson, L., Oltmanns, M., Hunter, W., Lloyd-Hartley, H., Kent, E., Rabe, B., Renshaw, R., 2023. The impacts of climate change on sea temperature around the UK and Ireland. *MCCIP Sci. Rev.* 1–18.
- de Nooijer, L.J., Toyofuku, T., Kitazato, H., 2009. Foraminifera promote calcification by elevating their intracellular pH. *Proc. Natl. Acad. Sci.* 106, 15374–15378.
- de Nooijer, L.J., Spero, H.J., Erez, J., Bijma, J., Reichart, G.J., 2014. Biomineralization in perforate foraminifera. *Earth Sci. Rev.* 135, 48–58.
- Dissard, D., Nehrke, G., Reichart, G.J., Bijma, J., 2010. The impact of salinity on the Mg/Ca and Sr/Ca ratio in the benthic foraminifera *Ammonia tepida*: results from culture experiments. *Geochim. Cosmochim. Acta* 74, 928–940.
- Dolman, A.M., Laepple, T., 2018. Sedprox: a forward model for sediment-archived climate proxies. *Clim. Past* 14, 1851–1868.
- Duenas-Bohórquez, A., Raitzsch, M., de Nooijer, L.J., Reichart, G.-J., 2011. Independent impacts of calcium and carbonate ion concentration on Mg and Sr incorporation in cultured benthic foraminifera. *Mar. Micropaleontol.* 81, 122–130.
- Elderfield, H., Bertram, C.J., Erez, J., 1996. A biomineralization model for the incorporation of trace elements into foraminiferal calcium carbonate. *Earth Planet. Sci. Lett.* 142, 409–423.
- Elderfield, H., Yu, J., Anand, P., Kiefer, T., Nyland, B., 2006. Calibrations for benthic foraminiferal Mg/Ca paleothermometry and the carbonate ion hypothesis. *Earth Planet. Sci. Lett.* 250, 633–649.
- Erez, J., 1978. Vital effect on stable-isotope composition seen in foraminifera and coral skeletons. *Nature* 273, 199–202.
- Fehrenbacher, J., Marchitto, T., Spero, H.J., 2020. Comparison of Laser Ablation and Solution-based ICP-MS results for Individual Foraminifer Mg/Ca and Sr/Ca analyses. *Geochem. Geophys. Geosyst.* 21 e2020GC009254.
- Fehrenbacher, J.S., Hupp, B.N., Branson, O., Evans, D., Foster, G.L., Glock, N., Thirumalai, K., Wycech, J., 2024. Individual foraminiferal analysis: A review of current and emerging geochemical techniques. *J. Foraminif. Res.* 54, 312–331.
- Fietzke, J., Anagnostou, E., 2023. Sources of inaccuracy in boron isotope measurement using LA-MC-ICP-MS. *Geostand. Geoanal. Res.* 47, 481–492.
- Findlay, H., Artioli, Y., Greenwood, N., Hartman, S., Flohr, A., León, P., Stiasny, M., Cronin, M., 2025. Ocean acidification around the UK and Ireland. *MCCIP Sci. Rev.* 1–31.
- Foster, G.L., Rae, J.W.B., 2016. Reconstructing Ocean pH with boron isotopes in foraminifera. *Annu. Rev. Earth Planet. Sci.* 44, 207–237.
- Foster, G.L., Pogge von Strandmann, P.A.E., Rae, J.W.B., 2010. Boron and magnesium isotopic composition of seawater. *Geochem. Geophys. Geosyst.* 11, Q08015.
- Foster, G.L., Hönisch, B., Paris, G., Dwyer, G.S., Rae, J.W., Elliott, T., Gaillardet, J., Hemming, N.G., Louvat, P., Vengosh, A., 2013. Interlaboratory comparison of boron isotope analyses of boric acid, seawater and marine CaCO₃ by MC-ICPMS and NTIMS. *Chem. Geol.* 358, 1–14.
- François, D., Reichart, G.-J., de Nooijer, L.J., 2025. Open or closed: pH modulation and calcification by foraminifera. *Sci. Adv.* 11, eadq8425.
- Gabitov, R.I., Sadekov, A., Leinweber, A., 2014. Crystal growth rate effect on Mg/Ca and Sr/Ca partitioning between calcite and fluid: an in situ approach. *Chem. Geol.* 367, 70–82.
- Gagnon, A.C., Gothmann, A.M., Branson, O., Rae, J.W.B., Stewart, J.A., 2021. Controls on boron isotopes in a cold-water coral and the cost of resilience to ocean acidification. *Earth Planet. Sci. Lett.* 554, 116662.
- Gallegos, A., 1996. Descriptive physical oceanography of the Caribbean Sea. In: Maul, G. A. (Ed.), *Small Islands: Marine Science and Sustainable Development*. Geophysical Union, Washington, DC, pp. 36–55.
- Gattuso, J.-P., Epitalon, J.-M., Lavigne, H., Orr, J., 2021. Seacarb: Seawater carbonate chemistry. R package version 3.3.0.
- Gutjahr, M., Bordier, L., Douville, E., Farmer, J., Foster, G.L., Hathorne, E.C., Hönisch, B., Lemarchand, D., Louvat, P., McCulloch, M., Noireaux, J., Pallavicini, N., Rae, J.W.B., Rodushkin, I., Roux, P., Stewart, J.A., Thil, F., You, C.-F., 2021. Sub-permil interlaboratory consistency for solution-based boron isotope analyses on marine carbonates. *Geostand. Geoanal. Res.* 45, 59–75.
- Hart, M., Molina, G., Smart, C., Widdicombe, C., 2016. The Western Channel Observatory: Benthic foraminifera in the plankton following storms. *Geosci. South-West Engl.* 14, 39–45.
- Healey, S.L., Thunell, R.C., Corliss, B.H., 2008. The Mg/Ca-temperature relationship of benthic foraminiferal calcite: New core-top calibrations in the <4°C temperature range. *Earth Planet. Sci. Lett.* 272, 523–530.
- Hohenegger, J., 2018. Foraminiferal growth and test development. *Earth Sci. Rev.* 185, 140–162.
- Holbourn, A., Henderson, A.S., MacLeod, N., 2013. A to V Atlas of Benthic Foraminifera. John Wiley & Sons 15–615.
- Holland, K., Eggins, S.M., Hönisch, B., Haynes, L.L., Branson, O., 2017. Calcification rate and shell chemistry response of the planktic foraminifer *Orbulina universa* to changes in microenvironment seawater carbonate chemistry. *Earth Planet. Sci. Lett.* 464, 124–134.
- Howes, E.L., Kaczmarek, K., Raitzsch, M., Mewes, A., Bijma, N., Horn, I., Misra, S., Gattuso, J.P., Bijma, J., 2017. Decoupled carbonate chemistry controls on the incorporation of boron into *Orbulina universa*. *Biogeosciences* 14, 415–430.
- Huber, M., Caballero, R., 2011. The early Eocene equable climate problem revisited. *Clim. Past* 7, 603–633.
- Hull, P.M., Franks, P.J.S., Norris, R.D., 2011. Mechanisms and models of iridium anomaly shape across the Cretaceous–Paleogene boundary. *Earth Planet. Sci. Lett.* 301, 98–106.
- Hülse, D., Vervoort, P., van de Velde, S.J., Kanzaki, Y., Boudreau, B., Arndt, S., Bottjer, D. J., Hoogakker, B., Kuderer, M., Middelburg, J.J., Volkenborn, N., Kirtland Turner, S., Ridgwell, A., 2022. Assessing the impact of bioturbation on sedimentary isotopic records through numerical models. *Earth Sci. Rev.* 234, 104213.
- Inglis, G.N., Bhatia, R., Evans, D., Zhu, J., Müller, W., Matthey, D., Thornalley, D.J.R., Stockey, R.G., Wade, B.S., 2023. Surface Ocean Cooling in the Eocene North Atlantic Coincides with declining Atmospheric CO₂. *Geophys. Res. Lett.* 50 e2023GL105448.
- Jia, Q., Zhang, S., Watkins, J.M., Devriendt, L.S., Huang, Y., Wang, G., 2024. Modeled foraminiferal calcification and strontium partitioning in benthic foraminifera helps reconstruct calcifying fluid composition. *Commun. Earth Environ.* 5, 36.
- Jiang, L.-Q., Carter, B.R., Feely, R.A., Lauvset, S.K., Olsen, A., 2019. Surface Ocean pH and buffer capacity: past, present and future. *Sci. Rep.* 9, 18624.
- Johnson, G.C., Purkey, S.G., 2009. Deep Caribbean Sea warming. *Deep-Sea Res. I Oceanogr. Res. Pap.* 56, 827–834.
- Kaczmarek, K., Langer, G., Nehrke, G., Horn, I., Misra, S., Janse, M., Bijma, J., 2015. Boron incorporation in the foraminifer *Amphistegina lessonii* under a decoupled carbonate chemistry. *Biogeosciences* 12, 1753–1763.
- Kirtland Turner, S., Hull, P.M., Kump, L.R., Ridgwell, A., 2017. A probabilistic assessment of the rapidity of PETM onset. *Nat. Commun.* 8, 353.
- Kisakürek, B., Eisenhauer, A., Böhm, F., Garbe-Schönberg, D., Erez, J., 2008. Controls on shell Mg/Ca and Sr/Ca in cultured planktonic foraminifera, *Globigerinoides ruber* (white). *Earth Planet. Sci. Lett.* 273, 260–269.
- Klochko, K., Kaufman, A.J., Yao, W., Byrne, R.H., Tossell, J.A., 2006. Experimental measurement of boron isotope fractionation in seawater. *Earth Planet. Sci. Lett.* 248, 276–285.
- Kozdon, R., Kelly, D.C., 2024. Hot tropical temperatures during the Paleocene-Eocene thermal Maximum revealed by paired *in situ* δ¹³C and Mg/Ca measurements on individual planktic foraminifer shells. *Paleoceanogr. Paleoclimatol.* 39 e2023PA004834.
- Kwiatkowski, L., Orr, J.C., 2018. Diverging seasonal extremes for ocean acidification during the twenty-first century. *Nat. Clim. Chang.* 8, 141–145.
- Langer, M.R., 1993. Epiphytic foraminifera. *Mar. Micropaleontol.* 20, 235–265.
- Lauvset, S.K., Lange, N., Tanhua, T., Bittig, H.C., Olsen, A., Kozyr, A., Álvarez, M., Azetsu-Scott, K., Brown, P.J., Carter, B.R., Cotrim da Cunha, L., Hoppema, M., Humphreys, M.P., Ishii, M., Jeansson, E., Murata, A., Müller, J.D., Pérez, F.F., Schirnick, C., Steinfeldt, R., Suzuki, T., Ulfso, A., Velo, A., Woosley, R.J., Key, R.M., 2024. The annual update GLODAPv2.2023: the global interior ocean biogeochemical data product. *Earth Syst. Sci. Data* 16, 2047–2072.
- Lear, C.H., Elderfield, H., Wilson, P.A., 2000. Cenozoic deep-sea temperatures and global ice volumes from Mg/Ca in benthic foraminiferal calcite. *Science* 287, 269–272.
- Lear, C.H., Mawbey, E.M., Rosenthal, Y., 2010. Cenozoic benthic foraminiferal Mg/Ca and Li/Ca records: toward unlocking temperatures and saturation states. *Paleoceanogr.* 25, A4215.
- Lisiecki, L.E., Raymo, M.E., 2005. A Pliocene-Pleistocene stack of 57 globally distributed benthic δ¹⁸O records. *Paleoceanogr.* 20, PA1003.
- Liu, H., Meyers, S.R., Marcott, S.A., 2021. Unmixing deep-sea paleoclimate records: A study on bioturbation effects through convolution and deconvolution. *Earth Planet. Sci. Lett.* 564, 116883.
- Lorens, R.B., 1981. Sr, Cd, Mn and Co distribution coefficients in calcite as a function of calcite precipitation rate. *Geochim. Cosmochim. Acta* 45, 553–561.
- Lutze, G., Thiel, H., 1989. Epibenthic foraminifera from elevated microhabitats: *Cibicides wuellerstorfi* and *Planulina ariminensis*. *J. Foraminif. Res.* 19, 153–158.
- Manley, C.J., 1997. Environmental Variables, Including Pollutants, Affecting Living Benthic foraminifera. University of Plymouth.
- Marchitto, T.M., Bryan, S.P., Curry, W.B., McCorkle, D.C., 2007. Mg/Ca temperature calibration for the benthic foraminifer *Cibicides pachyderma*. *Paleoceanogr.* 22, PA1203.
- Marshall, B.J., Thunell, R.C., Henehan, M.J., Astor, Y., Wejnert, K.E., 2013. Planktonic foraminiferal area density as a proxy for carbonate ion concentration: A calibration study using the Cariaco Basin ocean time series. *Paleoceanogr.* 28, 363–376.
- Mavromatis, V., Gautier, Q., Bosc, O., Schott, J., 2013. Kinetics of Mg partition and Mg stable isotope fractionation during its incorporation in calcite. *Geochim. Cosmochim. Acta* 114, 188–203.
- Mavromatis, V., Montouillout, V., Noireaux, J., Gaillardet, J., Schott, J., 2015. Characterization of boron incorporation and speciation in calcite and aragonite from co-precipitation experiments under controlled pH, temperature and precipitation rate. *Geochim. Cosmochim. Acta* 150, 299–313.
- Mayk, D., Fietzke, J., Anagnostou, E., Paytan, A., 2020. LA-MC-ICP-MS study of boron isotopes in individual planktonic foraminifera: A novel approach to obtain seasonal variability patterns. *Chem. Geol.* 531, 119351.
- McEvoy, A.J., Atkinson, A., Airs, R.L., Brittain, R., Brown, I., Fileman, E.S., Findlay, H.S., McNeill, C.L., Ostle, C., Smyth, T.J., Somerfield, P.J., Tait, K., Tarran, G.A., Thomas, S., Widdicombe, C.E., Woodward, E.M.S., Beesley, A., Conway, D.V.P., Fishwick, J., Haines, H., Harris, C., Harris, R., Hélaouët, P., Johns, D., Lindeque, P.K., Mesher, T., McQuatters-Gollop, A., Nunes, J., Perry, F., Queiros, A.M., Rees, A., Rühl, S., Sims, D., Torres, R., Widdicombe, S., 2023. The Western Channel Observatory: A century of physical, chemical and biological data compiled from pelagic and benthic habitats in the western English Channel. *Earth Syst. Sci. Data* 15, 5701–5737.

- Mellon, S., Kienast, M., Algar, C., de Menocal, P., Kienast, S.S., Marchitto, T.M., Moros, M., Thomas, H., 2019. Foraminifera Trace Anthropogenic CO₂ in the NW Atlantic by 1950. *Geophys. Res. Lett.* 46, 14683–14691.
- Mucci, A., Morse, J.W., 1983. The incorporation of Mg²⁺ and Sr²⁺ into calcite overgrowths: Influences of growth rate and solution composition. *Geochim. Cosmochim. Acta* 47, 217–233.
- Muller-Karger, F.E., Lorenzoni, L., Astor, Y.M., 2013. Partial Pressure (or Fugacity) of Carbon Dioxide, Dissolved Inorganic Carbon, pH, Alkalinity, Temperature, Salinity and Other Variables Collected from Discrete Sample, Profile and Time Series Profile Observations Using Alkalinity Titrator, CTD and Other Instruments from HERMANO GINES in the Caribbean Sea from 1995-11-08 to 2015-07-29 (NCEI Accession 0112926). NOAA National Centers for Environmental Information, Dataset.
- Noireaux, J., Mavromatis, V., Gaillardet, J., Schott, J., Montouillout, V., Louvat, P., Rollion-Bard, C., Neuvill, D.R., 2015. Crystallographic control on the boron isotope paleo-pH proxy. *Earth Planet. Sci. Lett.* 430, 398–407.
- Ostle, C., Williamson, P., Artioli, Y., Bakker, D.C., Birchenough, S., Davis, C.E., Dye, S., Edwards, M., Findlay, H.S., Greenwood, N., 2016. Carbon dioxide and ocean acidification observations in UK waters. Synthesis report with a focus on 2010–2015, 1–42.
- Paton, C., Hellstrom, J., Paul, B., Woodhead, J., Hergt, J., 2011. Iolite: Freeware for the visualisation and processing of mass spectrometric data. *J. Anal. At. Spectrom.* 26, 2508–2518.
- Pisano, A., Marullo, S., Artale, V., Falcini, F., Yang, C., Leonelli, F.E., Santoleri, R., Buongiorno Nardelli, B., 2020. New evidence of Mediterranean climate change and variability from sea surface temperature observations. *Remote Sens.* 12, 132.
- Quillmann, U., Marchitto, T.M., Jennings, A.E., Andrews, J.T., Friestad, B.F., 2012. Cooling and freshening at 8.2 ka on the NW Iceland Shelf recorded in paired δ¹⁸O and Mg/Ca measurements of the benthic foraminifer *Cibicides lobatulus*. *Quat. Res.* 78, 528–539.
- Rae, J.W.B., Foster, G.L., Schmidt, D.N., Elliott, T., 2011. Boron isotopes and B/Ca in benthic foraminifera: Proxies for the deep ocean carbonate system. *Earth Planet. Sci. Lett.* 302, 403–413.
- Raitzsch, M., Hathorne, E.C., Kuhnert, H., Groeneveld, J., Bickert, T., 2011. Modern and late Pleistocene B/Ca ratios of the benthic foraminifer *Planulina wuellerstorfi* determined with laser ablation ICP-MS. *Geology* 39, 1039–1042.
- Raitzsch, M., Rollion-Bard, C., Horn, I., Steinhofel, G., Benthien, A., Richter, K.U., Buisson, M., Louvat, P., Bijma, J., 2020. Technical note: Single-shell δ¹¹B analysis of *Cibicoides wuellerstorfi* using femtosecond laser ablation MC-ICPMS and secondary ion mass spectrometry. *Biogeosciences* 17, 5365–5375.
- Reimer, P.J., Reimer, R.W., 2001. A Marine Reservoir Correction Database and On-Line Interface. *Radiocarbon* 43, 461–463.
- Rollion-Bard, C., Erez, J., 2010. Intra-shell boron isotope ratios in the symbiont-bearing benthic foraminifer *Amphistegina lobifera*: Implications for δ¹¹B vital effects and paleo-pH reconstructions. *Geochim. Cosmochim. Acta* 74, 1530–1536.
- Rollion-Bard, C., Chausson, M., France-Lanord, C., 2003. pH control on oxygen isotopic composition of symbiotic corals. *Earth Planet. Sci. Lett.* 215, 275–288.
- Ruela, R., Sousa, M.C., deCastro, M., Dias, J.M., 2020. Global and regional evolution of sea surface temperature under climate change. *Glob. Planet. Chang.* 190, 103190.
- Sadekov, A., Lloyd, N.S., Misra, S., Trotter, J., D'Olivo, J., McCulloch, M., 2019. Accurate and precise microscale measurements of boron isotope ratios in calcium carbonates using laser ablation multicollector-ICPMS. *J. Anal. At. Spectrom.* 34, 550–560.
- Salmon, K.H., Anand, P., Sexton, P.F., Conte, M., 2016. Calcification and growth processes in planktonic foraminifera complicate the use of B/Ca and U/Ca as carbonate chemistry proxies. *Earth Planet. Sci. Lett.* 449, 372–381.
- Santos, G.M., Moore, R.B., Southon, J.R., Griffin, S., Hinger, E., Zhang, D., 2007. AMS ¹⁴C Sample Preparation at the KCCAMS/UCI Facility: Status Report and Performance of Small Samples. *Radiocarbon* 49, 255–269.
- Schmidt, M.W., Spero, H.J., Lea, D.W., 2004. Links between salinity variation in the Caribbean and North Atlantic thermohaline circulation. *Nature* 428, 160–163.
- Schmiedl, G., Pfeilsticker, M., Hemleben, C., Mackensen, A., 2004. Environmental and biological effects on the stable isotope composition of recent deep-sea benthic foraminifera from the western Mediterranean Sea. *Mar. Micropaleontol.* 51, 129–152.
- Schmittner, A., Bostock, H.C., Cartapanis, O., Curry, W.B., Filipsson, H.L., Galbraith, E. D., Gottschalk, J., Herguera, J.C., Hoogakker, B., Jaccard, S.L., Lisiecki, L.E., Lund, D.C., Martínez-Méndez, G., Lynch-Stieglitz, J., Mackensen, A., Michel, E., Mix, A.C., Oppo, D.W., Peterson, C.D., Repschläger, J., Sikes, E.L., Spero, H.J., Waelbroeck, C., 2017. Calibration of the carbon isotope composition (δ¹³C) of benthic foraminifera. *Paleoceanogr* 32, 512–530.
- Schweizer, M., Pawlowski, J., Kouwenhoven, T., van der Zwaan, B., 2009. Molecular phylogeny of common *Cibicidids* and related *Rotaliida* (foraminifera) based on small subunit rDNA sequences. *J. Foraminif. Res.* 39, 300–315.
- Sims, R.P., Bedington, M., Schuster, U., Watson, A.J., Kitidis, V., Torres, R., Findlay, H.S., Fishwick, J.R., Brown, I., Bell, T.G., 2022. Tidal mixing of estuarine and coastal waters in the western English Channel is a control on spatial and temporal variability in seawater CO₂. *Biogeosciences* 19, 1657–1674.
- Southon, J., Santos, G., Druffel-Rodriguez, K., Druffel, E., Trumbore, S., Xu, X., Griffin, S., Ali, S., Mazon, M., 2004. The Keck Carbon Cycle AMS Laboratory, University of California, Irvine: initial operation and a Background Surprise. *Radiocarbon* 46, 41–49.
- Standish, C.D., Chalk, T.B., Babila, T.L., Milton, J.A., Palmer, M.R., Foster, G.L., 2019. The effect of matrix interferences on in situ boron isotope analysis by laser ablation multi-collector inductively coupled plasma mass spectrometry. *Rapid Commun. Mass Spectrom.* 33, 959–968.
- Standish, C.D., Trend, J., Kleboe, J., Chalk, T.B., Mahajan, S., Milton, J.A., Page, T.M., Robinson, L.F., Stewart, J.A., Foster, G.L., 2024. Correlative geochemical imaging of *Desmophyllum dianthus* reveals biomineralisation strategy as a key coral vital effect. *Sci. Rep.* 14, 11121.
- Standish, C.D., Milton, J.A., Brown, R.M., Foster, G.L., 2025. Matrix independent and interference free in situ boron isotope analysis by laser ablation MC-ICP-MS/MS. *J. Anal. At. Spectrom.* 40, 1309–1322.
- Tang, J., Köhler, S.J., Dietzel, M., 2008. Sr²⁺/Ca²⁺ and ⁴⁴Ca/⁴⁰Ca fractionation during inorganic calcite formation: I. Sr incorporation. *Geochim. Cosmochim. Acta* 72, 3718–3732.
- Tesoriero, A.J., Pankow, J.F., 1996. Solid solution partitioning of Sr²⁺, Ba²⁺, and Cd²⁺ to calcite. *Geochim. Cosmochim. Acta* 60, 1053–1063.
- Thirumalai, K., Partin, J.W., Jackson, C.S., Quinn, T.M., 2013. Statistical constraints on El Niño Southern Oscillation reconstructions using individual foraminifera: A sensitivity analysis. *Paleoceanogr* 28, 401–412.
- Thompson, D.W.J., Wallace, J.M., Kennedy, J.J., Jones, P.D., 2010. An abrupt drop in Northern Hemisphere sea surface temperature around 1970. *Nature* 467, 444–447.
- Tierney, J.E., Judd, E.J., Osman, M.B., King, J.M., Truax, O.J., Steiger, N.J., Amrhein, D. E., Anchukaitis, K.J., 2025. Advances in Paleoclimate Data Assimilation. *Annu. Rev. Earth Planet. Sci.* 53, 625–650.
- Tindall, J.C., Haywood, A.M., Salzmann, U., Dolan, A.M., Fletcher, T., 2022. The warm winter paradox in the Pliocene northern high latitudes. *Clim. Past* 18, 1385–1405.
- Toyofuku, T., Matsuo, M.Y., de Nooijer, L.J., Nagai, Y., Kawada, S., Fujita, K., Reichart, G.-J., Nomaki, H., Tsuchiya, M., Sakaguchi, H., Kitazato, H., 2017. Proton pumping accompanies calcification in foraminifera. *Nat. Commun.* 8, 14145.
- Tripati, A., Elderfield, H., 2005. Deep-sea temperature and circulation changes at the Paleocene-Eocene Thermal Maximum. *Science* 308, 1894–1898.
- Trudgill, M., Nuber, S., Block, H.E., Crumpton-Banks, J., Jurikova, H., Little, E., Shankle, M., Xu, C., Steele, R.C.J., Rae, J.W.B., 2024. A simple, low-blank batch purification method for high-precision boron isotope analysis. *Geochim. Geophys. Geosyst.* 25 e2023GC011350.
- Westerhold, T., Marwan, N., Drury, A.J., Liebrand, D., Agnini, C., Anagnostou, E., Barnet, J.S.K., Bohaty, S.M., De Vleeschouwer, D., Florindo, F., Frederichs, T., Hodell, D.A., Holbourn, A.E., Kroon, D., Lauretano, V., Littler, K., Lourens, L.J., Lyle, M., Pälike, H., Röhl, U., Tian, J., Wilkens, R.H., Wilson, P.A., Zachos, J.C., 2020. An astronomically dated record of Earth's climate and its predictability over the last 66 million years. *Science* 369, 1383–1387.
- Wissiak, M., Rüggeberg, A., 2006. Colonisation and bioerosion of experimental substrates by benthic foraminifera from euphotic to aphotic depths (Kosterfjord, SW Sweden). *Facies* 52, 1–17.
- Worrall, F., Jarvie, H.P., Howden, N.J.K., Burt, T.P., 2016. The fluvial flux of total reactive and total phosphorus from the UK in the context of a national phosphorus budget: comparing UK river fluxes with phosphorus trade imports and exports. *Biogeochemistry* 130, 31–51.
- Yu, J., Elderfield, H., 2008. Mg/Ca in the benthic foraminifera *Cibicoides wuellerstorfi* and *Cibicoides mundulus*: Temperature versus carbonate ion saturation. *Earth Planet. Sci. Lett.* 276, 129–139.
- Yu, J., Foster, G.L., Elderfield, H., Broecker, W.S., Clark, E., 2010. An evaluation of benthic foraminiferal B/Ca and δ¹¹B for deep ocean carbonate ion and pH reconstructions. *Earth Planet. Sci. Lett.* 293, 114–120.
- Zachos, J.C., Bohaty, S.M., John, C.M., McCarren, H., Kelly, D.C., Nielsen, T., 2007. The palaeocene–Eocene carbon isotope excursion: constraints from individual shell planktonic foraminifer records. *Philos. Trans. R. Soc. A Math. Phys. Eng. Sci.* 365, 1829–1842.
- Zeebe, R.E., Wolf-Gladrow, D.A., Bijma, J., Hönisch, B., 2003. Vital effects in foraminifera do not compromise the use of δ¹¹B as a paleo-pH indicator: evidence from modeling. *Paleoceanogr* 18, 1043.
- Zeebe, R.E., Bijma, J., Hönisch, B., Sanyal, A., Spero, H.J., Wolf-Gladrow, D.A., 2008. Vital effects and beyond: A modelling perspective on developing palaeoceanographic proxy relationships in foraminifera. In: N., A.W.E., H., J.R. (Ed.), *Biogeochemical Controls on Palaeoceanographic Environmental Proxies*. Geological Society, London, pp. 45–58.